

SAND76-0581

Unlimited Release

UC-60

# Sandia Vertical-Axis Wind Turbine Project Technical Quarterly Report April-June 1976

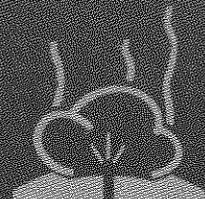
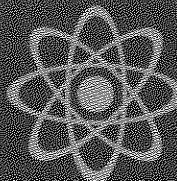
Advanced Energy Projects Division

Prepared by Sandia Laboratories, Albuquerque, New Mexico 87115  
and Livermore, California 94550 for the United States Energy Research  
and Development Administration under Contract AT(29-1)-789

Printed January 1977



Sandia Laboratories  
energy report



Issued by Sandia Laboratories, operated for the United States Energy Research & Development Administration by Sandia Corporation.

---

#### NOTICE

This report was prepared as an account of work sponsored by the United States Government. Neither the United States nor the United States Energy Research & Development Administration, nor any of their employees, nor any of their contractors, subcontractors, or their employees, makes any warranty, express or implied, or assumes any legal liability or responsibility for the accuracy, completeness or usefulness of any information, apparatus, product or process disclosed, or represents that its use would not infringe privately owned rights.

SF 1004-DF (3-75)

Printed in the United States of America

Available from  
National Technical Information Service  
U. S. Department of Commerce  
5285 Port Royal Road  
Springfield, VA 22161

Price: Printed Copy \$5.00 ; Microfiche \$3.00

SAND76-0581  
Unlimited Release  
Printed January 1977

Distribution  
Category UC-60

SANDIA VERTICAL-AXIS WIND TURBINE PROJECT  
TECHNICAL QUARTERLY REPORT  
April-June 1976

Advanced Energy Projects Division 5715

Edited by

Robert C. Reuter, Jr.  
Advanced Energy Projects Division, 5715

Robert E. Sheldahl  
Aerothermodynamics Division, 1333  
Sandia Laboratories  
Albuquerque, NM 87115

ABSTRACT

This report summarizes activities within the Sandia Laboratories Vertical-Axis Wind Turbine Project that occurred during the fourth quarter of fiscal year 1976. Included are highlights for the quarter and status reports on activities in areas of systems studies aerodynamics, electrical systems, structures, and mechanical design. Subheadings in each section cover general development activities and activities related to the 17-meter turbine and the 5-meter turbine. Also included in this report is the program of the Sandia Vertical-Axis Wind Turbine Technology Workshop, a list of workshop attendees, and a list of project-related Sandia publications.

## FOREWORD AND ACKNOWLEDGMENTS

The work covered herein was performed by Sandia Laboratories under a contract administered by the Wind Energy Conversion Branch (Division of Solar Energy) of the Energy Research and Development Administration. The time period is April 1, 1976 to June 30, 1976. Previous work has been reported in Sandia Vertical-Axis Wind Turbine Program Technical Quarterly Report, October-December 1975, SAND76-0036, printed April 1976, and Sandia Vertical-Axis Wind Turbine Program Technical Quarterly Report, January-March 1976, SAND76-0338, printed August 1976. This report represents contributions from the following Sandia staff members:

J. F. Banas	R. C. Reuter
J. H. Biffle	R. Rodeman
B. F. Blackwell	R. E. Sheldahl
L. V. Feltz	W. N. Sullivan
R. D. Grover	A. F. Veneruso
E. G. Kadlec	L. I. Weingarten
D. W. Lobitz	

In addition, John Nightingale, a technical summer hire, contributed work on the turbine braking system.

The following Sandia personnel contributed significantly to hardware development for the project:

K. G. Grant	R. S. Rusk
C. E. Longfellow	J. Lackey

A major international event which took place during this reporting period was the Vertical-Axis Wind Turbine Technology Workshop, held in Albuquerque, New Mexico, May 17-20, 1976. The proceedings of the workshop were published under the same title in Sandia report SAND76-5586.

## SUMMARY

The basic Darrieus vertical-axis wind turbine (VAWT) consists of fixed-pitch blades attached to a central, torque-transmitting shaft. Preliminary investigations of this device have noted a number of potential advantages over conventional horizontal-axis systems. These advantages provided the motivation for establishing a project at Sandia to investigate the feasibility of this turbine, particularly when used as an augmenting device to pump energy into an existing synchronous electrical network.

Based on the strategy that feasibility can best be established through a balanced program of hardware and analytical development, a twofold interactive technical approach has been adopted. This approach involves (1) development of the necessary analyses and empirical experience to design large, megawatt-range turbine systems that are economically optimized and (2) the use of this technical background in conjunction with the experience and manufacturing facilities of private industry to design and construct a series of large VAWT power-generating systems. This series will begin with a 17-meter-diameter turbine connected to a 60-kW synchronous generator.

Highlights of program activities and progress for the quarter, April-June 1976, are as follows:

- An assessment of relative energy output for synchronous and asynchronous operation has been made. Relative energy output was quantified by studying the influence of several power coefficient parameters.
- The influence of turbine diameter-to-height ratio on aerodynamic performance was investigated. For values of this ratio between  $2/3$  and 1, there appear to be no aerodynamic advantages or disadvantages to guide its selection.
- Aeroelastic analyses were performed by Prof. N. D. Ham (Sandia consultant) which indicate no potential blade flutter problem exists with the 17-meter turbine when the struts are in place. Blade cross section mass balancing was found analytically to be unimportant in contributing to the presence of blade instabilities.
- Several design features of the blades being evaluated and fabricated under contract by Kaman Aerospace Corporation for the 17-meter turbine were finalized. A new delivery schedule was determined which places completion of nonrecurring engineering by July 16, 1976, completion of tooling by September 7, 1976, and blade delivery by December 15, 1976.
- Comparison of blade airloads for the 17-meter turbine, as predicted by Sandia and Kaman, were made. Some differences in airload magnitudes were discovered.

- A summary of experimental data collected over the two previous quarters on the aerodynamic performance of the 5-meter turbine was made.
- Structural evaluation and design of numerous major components of the 17-meter turbine have been completed. These components include the support base, blade support tower, turbine tie-down elements and the braking system.

The main body of this report contains expanded discussions of progress made on program activities during the April-June 1976 quarter. Major headings of Systems Studies, Aerodynamics, Electrical Systems, Structures and Mechanical Design may each contain subsections on general development, 17-meter turbine activities and 5-meter turbine activities.

A major activity which took place during this quarter was the Sandia sponsorship of participation in the Vertical-Axis Wind Turbine Workshop held May 17-20, 1976, in Albuquerque, NM. Sections VI and VII of this report contain the workshop program and attendance list, respectively.

Section VIII contains an updated list of Sandia publications and presentations, except those related to the workshop, which are contained in Section VI. The final section of the report, Section IX, contains a list of references.

## CONTENTS

		<u>Page</u>
I	SYSTEM STUDIES	11
	Relative Energy Output From Synchronous and Asynchronous Operation	11
	Influence of Power Coefficient	11
	Influence of Diameter-to-Height Ratio on Turbine Design	15
II	AERODYNAMICS	18
	Aeroelastic Analysis	18
	Wind Tunnel Tests	18
	Aerodynamic Loads, 17 Meter	19
	Load Amplitude	20
	Rotational Angle Load Variations	23
	Summary and Concluding Remarks	23
	5 Meter Turbine Performance	24
	Test Set-Up	25
	Data Reduction	26
	Power Coefficients	29
III	ELECTRICAL SYSTEMS AUTOMATIC CONTROL AND DATA ACQUISITION	32
IV	STRUCTURES	35
	Modal Analysis	35
	Blade Buckling Studies, 17 Meter	35
	Suggested Method for Establishing Fatigue Life of 17 Meter VAWT Blades	36
	Turbine Base/Tower/Tiedown Components	39
	Turbine Tie-Down, 17 Meter	43
	Phase I Design Results	43
	Phase II Design, Initial Tension	44
V	MECHANICAL DESIGN	49
	Low Cost Blade Fabrication Studies	49
	Kaman 17 Meter Blade Contract	51
	Mechanical Design, 17 Meter	52
	Turbine Braking System, 17 Meter	54
	Turbine Response to Braking	54
	Mechanical Design	55
	Electrical Design	57
VI	VERTICAL-AXIS WIND TURBINE TECHNOLOGY WORKSHOP PROGRAM	61
VII	WORKSHOP ATTENDEES	63
VIII	SANDIA PUBLICATIONS AND PRESENTATIONS (APRIL-JUNE 1976)	70
IX	PREVIOUS SANDIA PUBLICATIONS AND PRESENTATIONS	71
X	REFERENCES	74

ILLUSTRATIONS

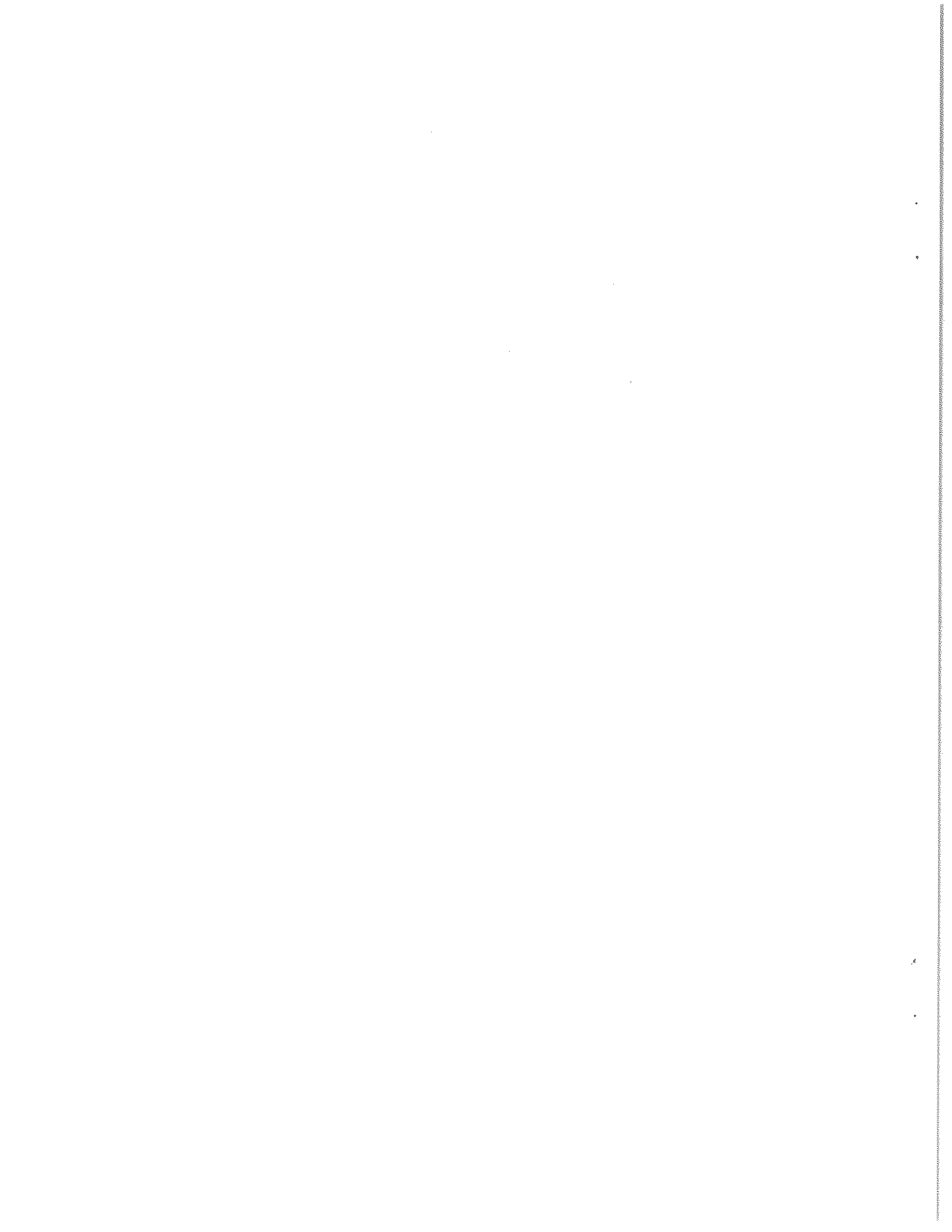
<u>Figure</u>		<u>Page</u>
1	Power Coefficient with Variable Parameters	12
2	Relative Difference in Energy Output for Single Speed Synchronous Operation	13
3	Relative Difference in Energy Output for Two-Speed Synchronous Operation	14
4	Relative Difference in Energy Output as a Function of Turbine Radius	15
5	$C_p$ Calculation with Wind Shear	17
6	Minimum Section Drag Coefficient as a Function of Reynolds Number for Four Symmetrical Airfoils	19
7	Aerodynamic Flap Load Comparison 30 MPH, 50 RPM	21
8	Aerodynamic Lead/Lag Load Comparison - 30 MPH, 50 RPM	21
9	Flap Force Comparison, 75 RPM, 80 MPH	22
10	Lead/Lag Load Comparison, 75 RPM, 80 MPH	22
11	Lead/Lag Load Variations at $R/R_{MAX} = 0.82$ , 50 RPM, 30 MPH	24
12	Lead/Lag Load Variations at Turbine - Beltline, 50 RPM, 30 MPH	24
13	The 5-m Turbine System	25
14	Sample Record of Torque and Wind Speed	26
15	Wind Speed Frequency Distribution, 87.5 RPM	27
16	Average Torque, 87.5 RPM	27
17	Wind Speed Frequency Distribution, 137.5 RPM	27
18	Average Torque, 137.5 RPM	27
19	Wind Speed Frequency Distribution, 150 RPM	28
20	Average Torque, 150 RPM	28
21	Wind Speed Frequency Distribution, 175 RPM	28
22	Average Torque, 175 RPM	28
23	Power Coefficient $C_p$ ( $Re = 2.6 \times 10^5$ )	30
24	Power Coefficient $C_p$ ( $Re = 4.0 \times 10^5$ )	30
25	Power Coefficient $C_p$ ( $Re = 4.4 \times 10^5$ )	30
26	Power Coefficient $C_p$ ( $Re = 5.1 \times 10^5$ )	30
27	Power Coefficient $K_p$ ( $Re = 2.6 \times 10^5$ )	30
28	Power Coefficient $K_p$ ( $Re = 4.0 \times 10^5$ )	30
29	Power Coefficient $K_p$ ( $Re = 4.4 \times 10^5$ )	31
30	Power Coefficient $K_p$ ( $Re = 5.1 \times 10^5$ )	31
31	Comparison of Theory and Data for 5 m Turbine at 175 RPM	31
32	Automatic Control of VAWT	32
33	Microprocessor Program Flowchart for VAWT	33
34	Block Diagrams of Wind Instrumentation Systems	34
35	Fatigue Strength vs Number of Cycles	37
36	Goodman Diagram, Extruded 6061-T6	38
37	Details of Turbine Base and Tower	40
38	Finite Element Model of Base/Tower/Tiedown System, 17 m Turbine	41
39	Cable Geometry	44

ILLUSTRATIONS (continued)

<u>Figure</u>		<u>Page</u>
40	Initial Tension vs Sag	45
41	Tension Change vs Deflection	46
42	Final Cable Tension vs Horizontal Tower Deflection and Cable Chord Length Change	47
43	Strike Point Sag vs Horizontal Tower Deflection and Cable Chord Length Change	48
44	Extruded Aluminum Blade	49
45	Blade with Roll-Formed Components	50
46	Braking Response Curves	55
47	Braking System Schematic	57
48	Proportional Brake Electrical System	58
49	Emergency Brake Electrical System	59
50	Brake Control Panel	60

TABLES

<u>Table</u>		<u>Page</u>
I	Blade Properties as Determined from Geometry Alone $S = 25.14$ m	16
II	Optimized Systems for Maximum Energy in 12 MPH Avg Wind Site, Fixed Blade Length, 25.14 m. Wind Shear Included	16
III	Unnotched Wrought 6061-T6	36
IV	Extruded 6061-T6	37
V	Load and Deflection Data - Tower and Bearings	42



SANDIA VERTICAL-AXIS WIND TURBINE PROJECT  
TECHNICAL QUARTERLY REPORT  
April-June 1976

I. SYSTEMS STUDIES

Relative Energy Output From Synchronous and Asynchronous Operation

The major thrust of Sandia's wind energy project has been directed toward development of large vertical-axis Darrieus wind turbines for utility grid applications.

It is planned to operate these turbines at constant rotational speed by connecting to an existing utility grid through a synchronous generator. The performance characteristics of current turbine designs had an influence on the decision to pursue this type of system. Specifically, the ability of the Darrieus turbine to self-regulate in the synchronous mode, thereby eliminating costly aerodynamic controls, is viewed as a definite advantage over more conventional turbines [1]. On the other hand, asynchronous operation, where the rotational speed is varied in proportion to the wind speed to maintain maximum efficiency, has the potential for greater energy output. It is important to determine the amount of improved energy production to judge the worth of systems of increased complexity.

This section summarizes an assessment of relative energy output for synchronous and asynchronous operation. A power coefficient with variable parameters is used to indicate the influence of the parameters on relative energy output.

For well-designed turbines the results indicate a difference in energy output of about 5 percent while for off-optimum designs the difference can be 30 percent. The benefit of using two fixed rotational speeds in synchronous operation is also examined. In this case, the difference in energy output can be reduced by 2 percent to 20 percent depending on the turbine design. Finally, since data indicate a strong dependence of power coefficient on Reynolds number, comparison of the two modes of operation is made with performance characteristics of current turbine designs. The difference is found to be about 10 percent to 20 percent; furthermore, the use of two fixed speeds only reduces this difference by about 1 percent.

Influence of Power Coefficient

In comparing the energy output from synchronous and asynchronous operation, the influence

of features of the power coefficient should be understood in order to identify improved turbine designs. Annual energy output has been calculated from a system model which uses a power coefficient with variable parameters.

The particular functional form for the power coefficient is shown in Figure 1. Features of interest are the maximum efficiency  $C_{p_{max}}$ , the tip speed ratio  $\lambda_m$  corresponding to maximum efficiency, the tip speed ratio  $\lambda_r$  at zero efficiency, the tip speed ratio  $\lambda_k$  at which power reaches a maximum with respect to wind speed, and an exponent  $n$ , which defines the turbine output power for wind speeds exceeding the rated wind speed. In addition, the system model accounts for the wind speed frequency distribution at a site as well as component efficiencies as a function of load.

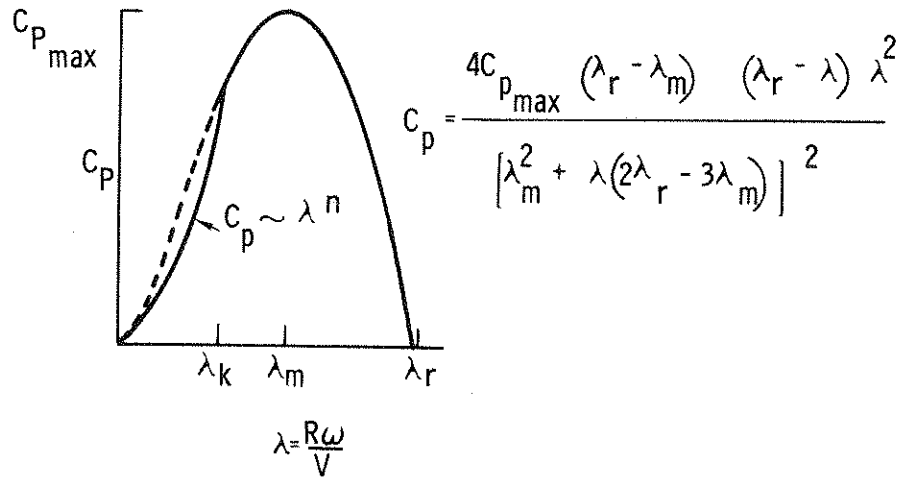


Figure 1. Power Coefficient with Variable Parameters

For synchronous operation, annual energy  $E_{sync}$  is proportional to  $C_{p_{max}}$  and is a function of  $R\omega/V$ ,  $\lambda_k/\lambda_m$ ,  $\lambda_r/\lambda_m$ , and  $n$ . These parameters also define the equipment ratings required to achieve self-regulation. The fixed rotational speed is chosen by selecting a value for  $R\omega/\lambda_m$ . If this value is low, the rated power is low and relatively little energy is produced. Alternatively, if this value is high, the rated power is high but corresponding wind speeds occur seldom and again relatively little energy is produced. There appears to be a value of  $R\omega/\lambda_m$  which maximizes  $E_{sync}$ . In the results to follow the rotational speed has been chosen to maximize annual energy.

For asynchronous operation below rated power, the tip speed is made to vary in proportion to the wind speed such that  $R\omega/V$  is equal to  $\lambda_m$ , that is, the turbine achieves maximum efficiency  $C_{p_{max}}$ . Annual energy  $E_{async}$  is proportional to  $C_{p_{max}}$  and is a function of  $P_{rated}/C_{p_{max}}$  where  $P_{rated}$  is the rated power. There appears to be a unique value of  $P_{rated}/C_{p_{max}}$  which maximizes  $E_{async}$ . In the results to follow, the rated power has been chosen to maximize annual energy.

It should be noted that this energy output represents an upper bound. For practical systems the tip speed will not track the wind speed precisely and therefore the turbine efficiency will not always be  $C_{p_{max}}$ .

Figure 2 shows the percentage difference between  $E_{async}$  and  $E_{sync}$  as a function of  $\lambda_k/\lambda_m$  and  $\lambda_r/\lambda_m$ . This difference is independent of  $C_{p_{max}}$  and  $\lambda_m$ . It is, however, desirable to achieve high values for these parameters. The value of  $C_{p_{max}}$  should be made high in order to increase the energy output using either operational mode. The value of  $\lambda_m$  should be made high in order to increase rotational speeds and thereby reduce the cost of the transmission and generating equipment.

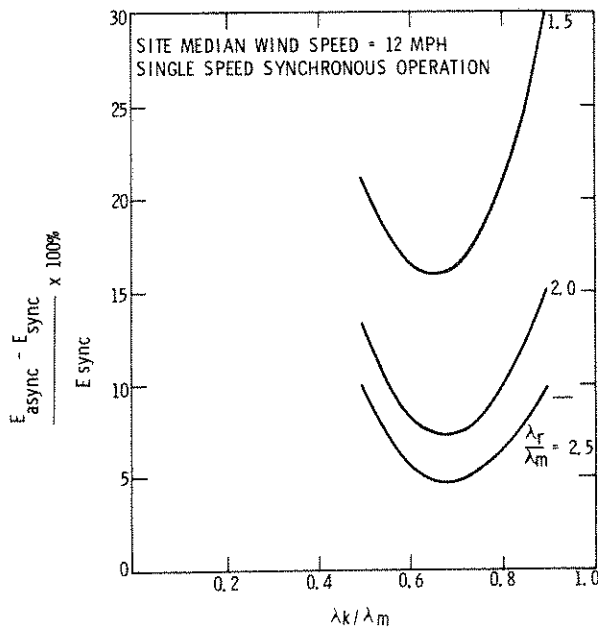


Figure 2.  
Relative Difference in Energy Output for Single Speed Synchronous Operation

For typical values of  $\lambda_k/\lambda_m$  and  $\lambda_r/\lambda_m$ , the energy outputs differ by 5 percent to 30 percent. The difference can be made small by making  $\lambda_r/\lambda_m$  large; that is the power coefficient curve is broadened. In this case, even though the rotational speed is fixed in synchronous operation, the turbine efficiency remains relatively high over a wide range of tip speed ratios and hence wind speeds. Figure 2 also indicates that the difference in energy output is minimized with respect to  $\lambda_k/\lambda_m$  at a value of about 0.7. A qualitative explanation for the occurrence of this minimum follows: If the value of  $\lambda_k/\lambda_m$  is low, the required rated power for synchronous operation is high and the decreased component efficiencies at reduced loads tend to give low energy output. If the value of  $\lambda_k/\lambda_m$  is high, the peak effective turbine efficiency is reduced and energy output is low. Thus, energy output is maximized for an intermediate value of  $\lambda_k/\lambda_m$ .

A potential improvement to energy output for synchronous operation can be made through the use of a multiple fixed speed transmission. Depending on the current wind speed, a

rotational speed which maximizes power would be selected from the available set. It should be noted, however, that for a practical system this procedure can only be approximated since speed changes could not be accomplished instantaneously. Figure 3 shows the difference in energy output as a function of  $\lambda_k/\lambda_m$  and  $\lambda_r/\lambda_m$  for two-speed synchronous operation. The availability of a second fixed rotational speed can reduce the difference by 2 percent to 20 percent.

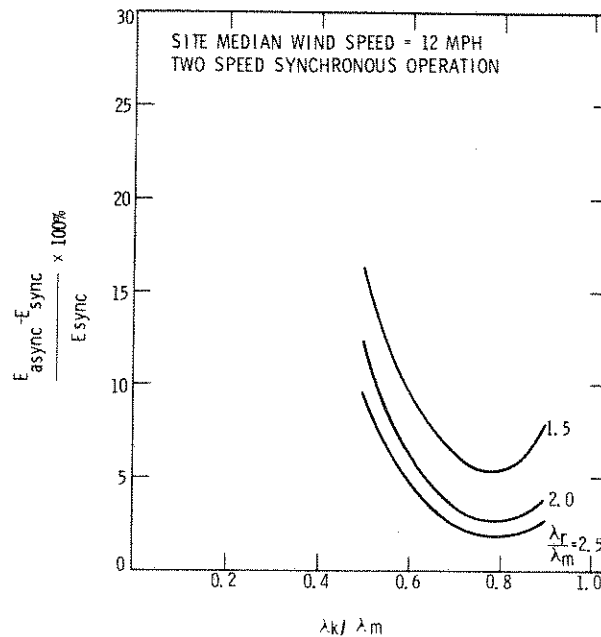


Figure 3. Relative Difference in Energy Output for Two-Speed Synchronous Operation

Wind tunnel test data and aerodynamic model predictions [2] indicate that the features of the power coefficient are substantially dependent on Reynolds number. For example, trends with increasing Reynolds number appear to be that  $C_{p_{max}}$  and  $\lambda_r/\lambda_m$  are increasing while  $\lambda_k/\lambda_m$  is decreasing. Because of these opposing tradeoffs in turbine performance characteristics, the effect of Reynolds number on relative energy output from synchronous and asynchronous operation is not immediately obvious using the previous results. Figure 4 shows this difference as a function of turbine radius when the effects of Reynolds number are included. For large turbines the difference is about 10 percent to 20 percent. It appears that the decrease in  $\lambda_k/\lambda_m$  with increasing Reynolds number (i.e., increasing turbine size) is the dominant factor in reducing energy output for synchronous operation. Figure 4 also indicates that for turbines of current design, the use of a second fixed rotational speed increases energy output by less than 1 percent.

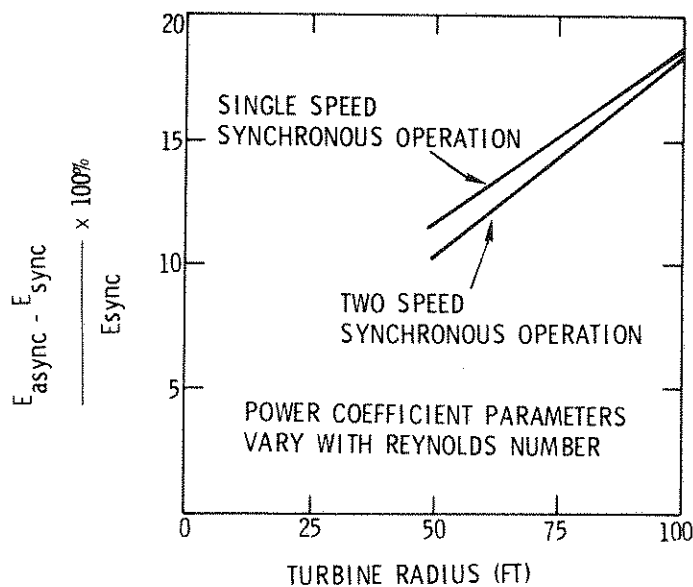


Figure 4. Relative Difference in Energy Output as a Function of Turbine Radius

#### Influence of Diameter-to-Height Ratio on Turbine Design

The previous works of Blackwell and Reis [3,4] have shown that the geometric characteristics of the troposkien can be expressed as a function of the diameter/height ratio ( $\beta$ ). Results from these studies indicate that  $\beta$  can be treated as a design parameter with a value chosen such that system energy costs are minimized. A parametric study was undertaken to investigate some of the aerodynamic, system, and structural implications of various turbine diameter/height ratios.

The baseline design chosen was a 3-bladed turbine with a diameter and height of 17 m (55.8 ft) NACA 0012 airfoil section, 0.5 m (19.7 in) chord, and 4.6 m (15 ft) ground clearance. For this configuration, the blade length was 25.1 m (82.5 ft). If the blade cross section remains fixed, then blade cost should be directly proportional to blade length. In order to facilitate comparison between the various diameter/height ratios, the blade length (and hopefully blade cost) was held constant. Table I presents the turbine geometrical characteristics that are dependent only on the parameter  $\beta$  (for a fixed blade length).

Since the ground clearance was assumed fixed at 4.6 m (15 ft), the velocity at the turbine centerline increases with decreasing  $\beta$ . Therefore, wind shear must be accounted for in the aerodynamic calculations. For the purpose of this analysis, the 1/7th power law was assumed valid. The aerodynamic performance for the five configurations in Table II was computed with a variable Reynolds number version of the Strickland [5] model, and the results are presented in Figure 5. Both the power production and tip speed have been normalized by a reference velocity ( $V_{ref}$ ) at 3.66 m/s (12 ft/s). The large values of the reference

power coefficient are due to the fact that the turbine sees an effective velocity much larger than the reference value of 3.66 m/s. The maximum value of the reference power coefficient and the speed ratio at which it occurs are a function of  $\beta$ . If maximum power production could be equated to minimum energy cost, one would choose  $\beta = 2/3$ . However, system and structural implications must also be considered.

TABLE I  
Blade Properties as Determined from Geometry Alone S = 25.14 m

$\beta = \frac{R_{\max}}{Z_{\max}}$	$Z_{\max}$ (m)	$R_{\max}$ (m)	$A_s$ (m <sup>2</sup> )
0.5	10.95	5.48	159.94
2/3	10.09	6.73	181.16
0.8	9.43	7.54	189.53
1.0	8.50	8.50	192.67
1.2	7.69	9.22	187.56

TABLE II  
Optimized Systems for Maximum Energy in 12 MPH Avg Wind Site,  
Fixed Blade Length, 25.14 m, Wind Shear Included

$\beta = \frac{R_{\max}}{Z_{\max}}$	P rated (kW)	Max Torque (ft-lbs)	$E_{\text{tot}}$ (kW-hr)/year	RPM
0.5	100	9,531	126,900	73.9
2/3	110	12,516	147,300	61.9
0.8	120	14,802	150,900	57.1
1.0	120	16,572	148,800	51.0
1.2	110	12,700	126,400	61.0

The structural implications are the most difficult to examine because resonant frequency and stress calculations generally require detailed modeling of the geometry. It is intuitively clear, however, that the low  $\beta$  designs would respond better to gravitational loadings,\* but buckling of the rotating shaft would be more severe because of increased length. Tie-down loads will be greater for the low  $\beta$  designs because the center of the turbine swept area is

\*The current Sandia 17-m design with  $\beta = 1$  is not dominated by gravitational loads, and their reduction would not be particularly beneficial for this turbine.

at a greater height and hence higher wind speed. The effect of  $\beta$  on other major stresses (due to centrifugal and aerodynamic loads) and the resonant frequencies remain to be investigated. It is doubtful that there will be a massive effect, structurally, on these performance measures, at least for  $\beta$  in the range of 0.66 to 1.2.

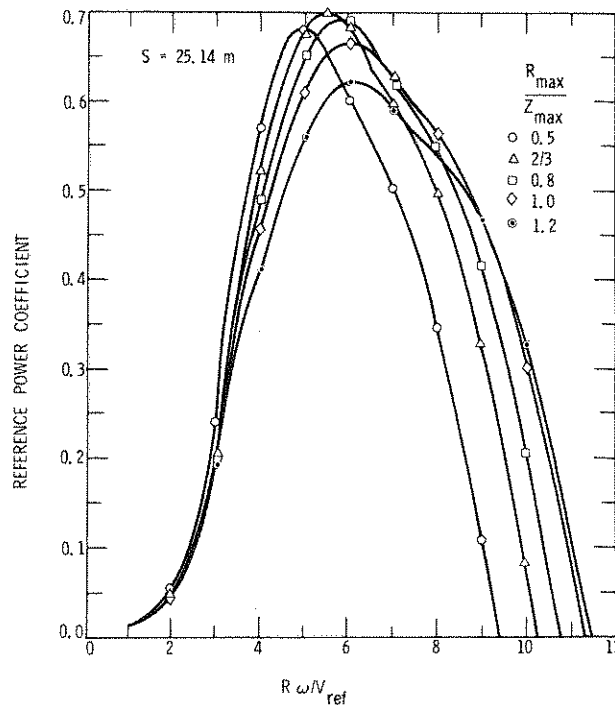


Figure 5.  $C_p$  Calculation with Wind Shear (Reference Velocity at 12 Feet Utilized)

A very practical reason for favoring a low  $\beta$  design is the ease of handling and shipping. Approximate size limitations on rail shipments in the United States are 3 m (10 ft) wide by 4.3 m (14 ft) high. These size constraints will limit the maximum size of a single blade segment.

In summary, it appears that there are no compelling aerodynamic performance advantages or disadvantages associated with any choice of  $\beta$  between 2/3 and 1.0. The low  $\beta$  turbine does have a higher rotational speed, however, which could lead to lower transmission costs. The structural tradeoffs associated with  $\beta$  are not clear, and more study is recommended in this area.

## II. AERODYNAMICS

### Aeroelastic Analysis

Dr. Norman D. Ham, Professor of Aeronautical Engineering, Massachusetts Institute of Technology, has been serving as a consultant in the area of aeroelasticity since December, 1975. The primary objective was to have Professor Ham analyze and evaluate the problem of aerodynamic flutter in the blades of the vertical axis wind turbine. An aeroelastic analysis of the stability of the coupled bending and torsional motion of the blades was performed, and numerical evaluations were made of estimated flutter speeds for the 2 meter wind tunnel model and the forthcoming 17 meter turbine. Estimates of the flutter speed for the 2 meter model agreed fairly well with those observed experimentally. Details of the analysis and numerical evaluations are contained in Reference [7]. The effect of intermediate support struts was included for evaluation of the 17 meter turbine, and it was shown that flutter speeds are expected to be approximately twice the maximum turbine operating speed.

Possibly one of the most valuable contributions of this work is the conclusion that blade cross-section mass balancing is relatively unimportant in contributing to the presence of flutter, compared to so called "Coriolis effects". Disregarding the necessity to mass balance blade cross-sections suggests cost savings in blade manufacturing. It is generally quite costly to insure that the blade cross-section's center of gravity, center of aerodynamic pressure, and elastic axis are coincident.

Additional work on numerical evaluation of flutter speeds and experimental verification of flutter speeds, parameter sensitivities and mass balancing is being planned.

### Wind Tunnel Tests

The data presented at the Vertical-Axis Wind Turbine Technology Workshop under the title "Aerodynamic Characteristics of Four Symmetrical Airfoil Sections Through 180 Degrees Angle of Attack at Low Reynolds Number (Preliminary Data Report)" was as the title indicates, preliminary. One aspect of the preliminary data about which the authors expressed concern was the drag data. The data presented had unusually low values of drag for the airfoil sections at low angles of attack. These data were reexamined, found to be in error, and were corrected. The corrected drag data are presented in Figure 6 which shows the minimum drag coefficient as a function of Reynolds number. The data for the NACA 0012 airfoil correspond very closely to published data in the Reynolds number range of  $0.7 \times 10^6$  to  $2.0 \times 10^6$ .

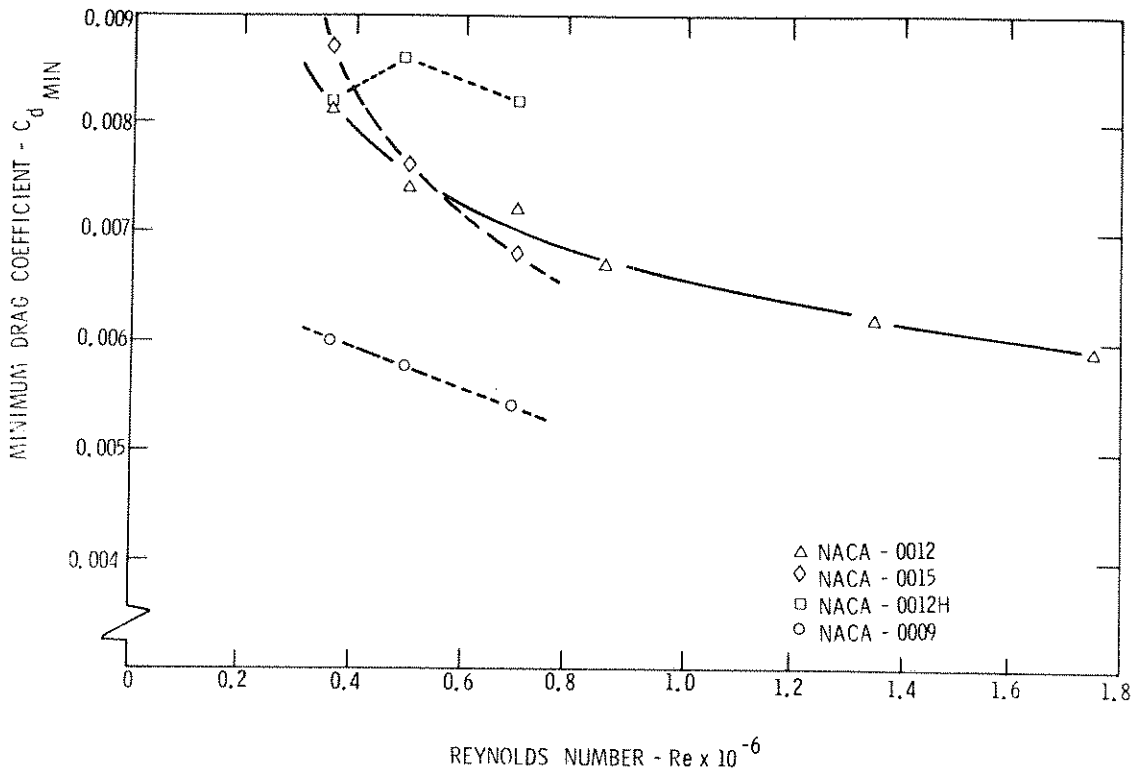


Figure 6. Minimum Section Drag Coefficient as a Function of Reynolds Number for Four Symmetrical Airfoils

Aerodynamic Loads, 17 Meter

During this quarter, efforts have been concentrated on comparing various aerodynamic load models which have been formulated for the Darrieus turbine. Of particular interest is a model developed by Kaman for their own analysis of the 17 m turbine. The other models used in the comparison are the single and multiple streamtube models which have been discussed in the first Technical Quarterly Report [2].

In summary, the major differences in the models concern the nature of the effective wind velocity which exists within the turbine. In the single streamtube model, a uniform velocity is assumed for the turbine interior with a magnitude calculated by balancing momentum with the net drag on the turbine. The Kaman model is similar to this except that a "bullet-shaped" interior velocity profile is assumed. This profile yields a minimum velocity at the center of the turbine projected area which increases as the edge of the projected area is approached. The parameters needed to quantify the profile are determined by effecting an overall momentum balance on the turbine. The multiple streamtube model considers the turbine interior to be made up of many individual streamtubes flowing parallel to the ambient wind vector. The interior velocity is then calculated by balancing momentum on each individual streamtube.

The following results show quite clearly that the different model assumptions can lead to substantial quantitative differences in the calculated blade loads. As none of the models are "exact" representations of the actual aerodynamics which occur, there is no apparent means to resolve the conflict in the short-term. While efforts will continue to determine the source of this conflict, our current approach is to consider the suitability of the 17 m design (particularly with regard to fatigue life) based on the upper and lower limits of predicted loads. The 17 m test program will be designed to establish experimentally which model or models are the most representative, so that future designs may be carried out using realistic load models.

### Load Amplitude

To compare load amplitude, data were supplied by Kaman on distributed loads along the blade for 50 rpm, 30 mph, and 75 rpm, 80 mph conditions. These loads are summarized in Figures 7 through 10 where the load distributions correspond to that particular turbine rotational angle which yields the largest force at the turbine centerline.

In Figure 7, the flap loading (normal to the flatwise plane of the blade) is given for four different analyses. Both the single and multiple streamtube models predict similar loads with the Kaman prediction being about 50% lower along the curved blade section. The single and multiple streamtube models used airfoil lift and drag data from Strickland's report [5] and these data differ somewhat from Kaman's. However, using Kaman's airfoil data in the single streamtube model does not change the results significantly, as shown in Figure 7.

In Figure 8, the differences in model predictions of lead/lag loads are more pronounced, particularly along the curved blade section. The Kaman loads in this region are less by about a factor of three from the single and multiple streamtube model predictions.

Figures 9 and 10 show an analogous comparison at 75 rpm, 80 mph. The agreement between models is reasonable for flap loads, with substantial disagreement shown for the lead/lag predictions. At this higher loading condition, the use of Kaman's airfoil data in the single streamtube model has more effect than in the 50 rpm, 30 mph case. This is due to the higher blade angles of attack (low tip speed ratio) associated with the 75 rpm, 80 mph analyses, as the Kaman and Strickland airfoil data differ most at high angles of attack.

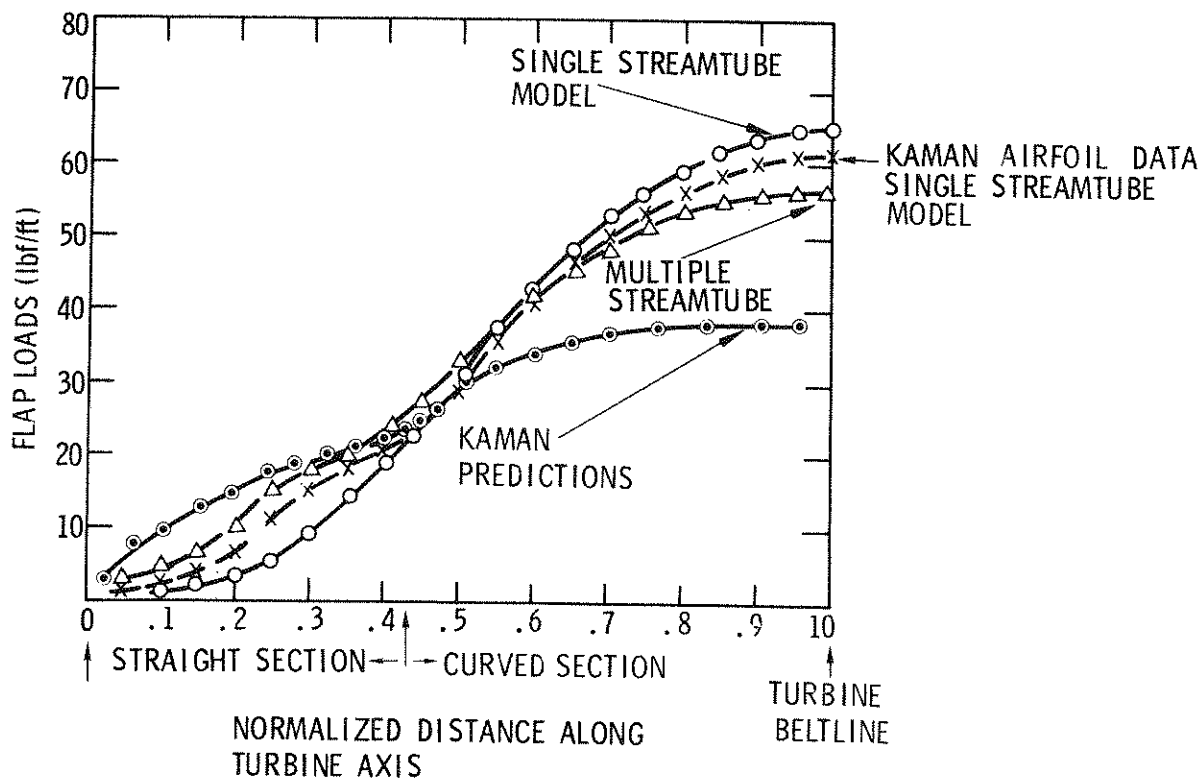


Figure 7. Aerodynamic Flap Load Comparison 30 MPH, 50 RPM

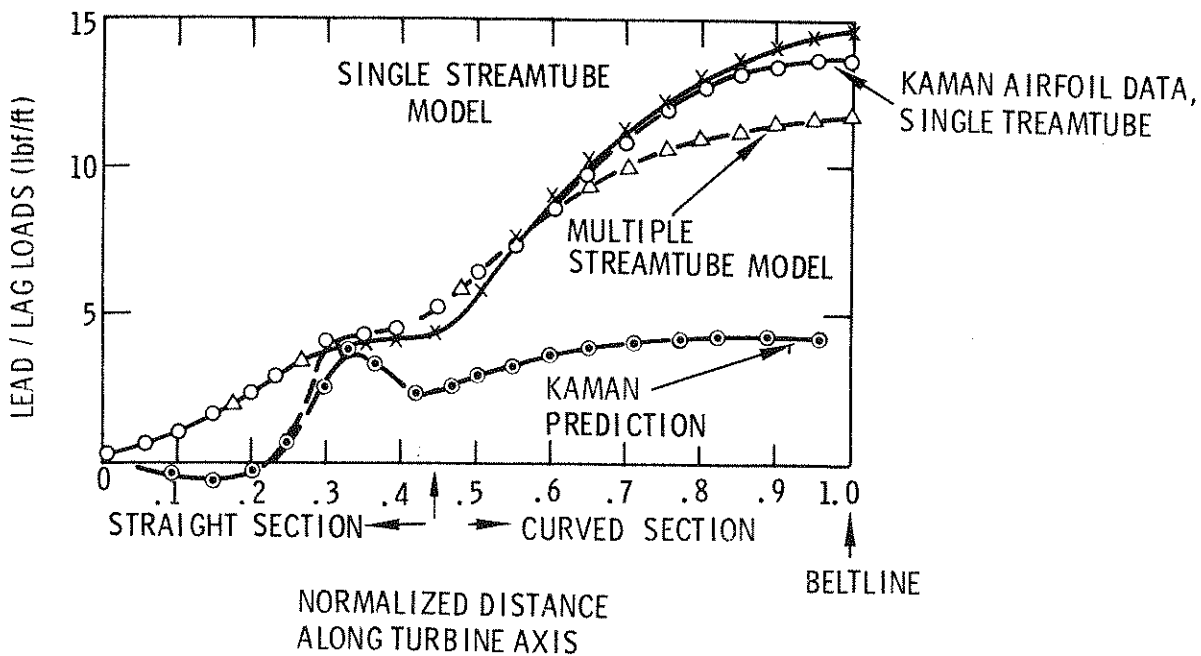


Figure 8. Aerodynamic Lead/Lag Load Comparison - 30 MPH, 50 RPM

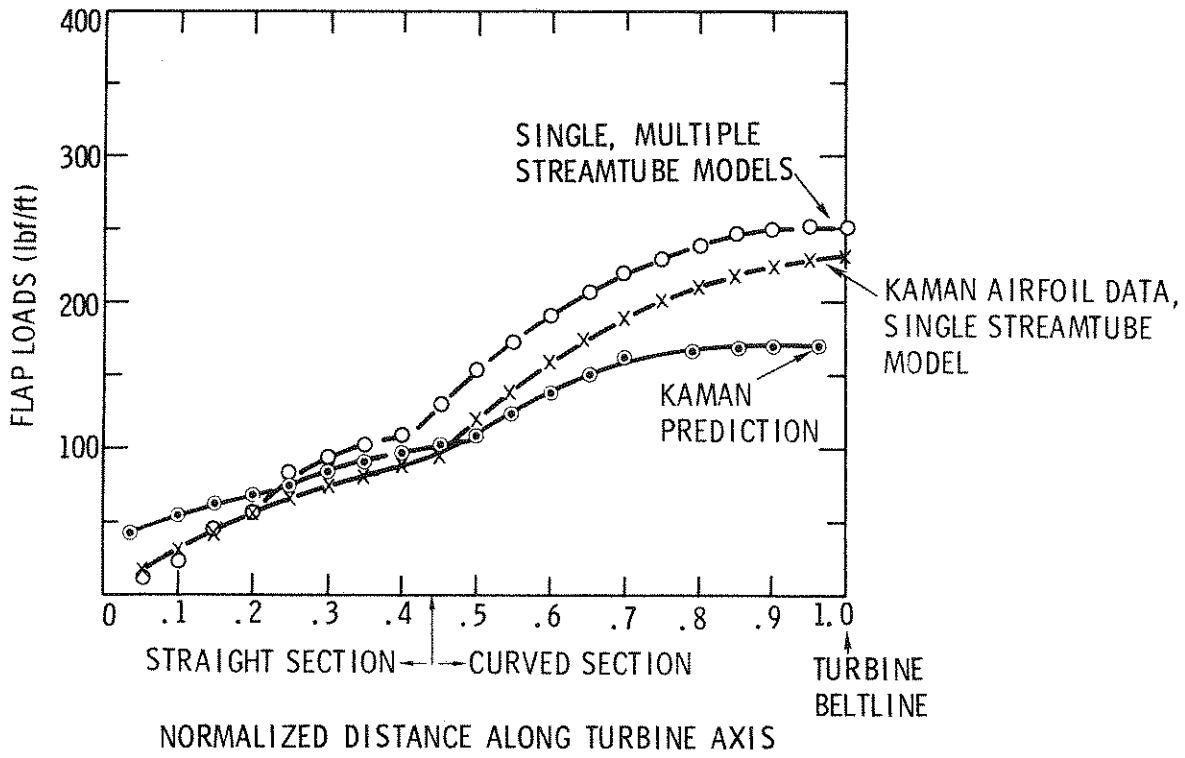


Figure 9. Flap Force Comparison, 75 RPM, 80 MPH

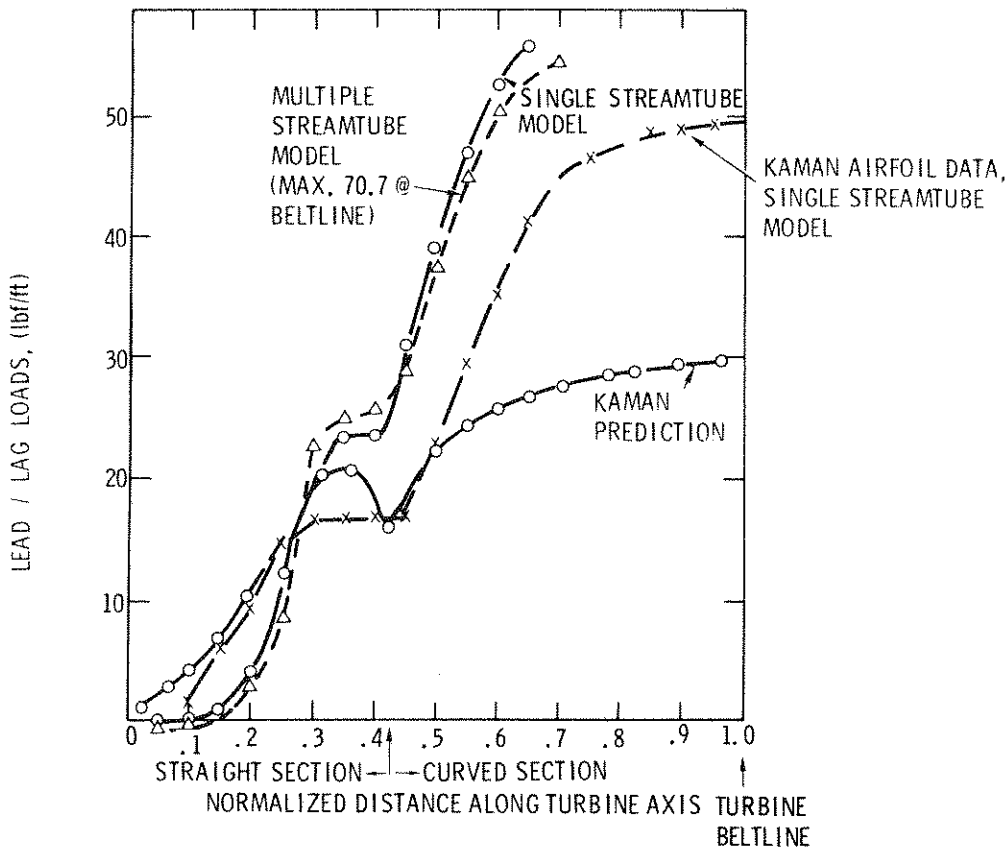


Figure 10. Lead/Lag Load Comparison, 75 RPM, 80 MPH

### Rotational Angle Load Variations

The variation of blade loads during turbine rotation is important in assessing the time-varying nature of aerodynamic loads. Kaman has supplied output from their model showing the rotational variation of lead/lag loads for the 50 rpm, 30 mph operating condition. Figure 11 shows their results along with a single streamtube load prediction for loads at the turbine equator. The most obvious difference is in the vicinity of the 90° rotational angle, where Kaman's loads are nearly zero while the single streamtube loads are a maximum. This is apparently due to the "bullet-shaped" interior velocity profile used by Kaman, which leads to a minimum interior velocity along the turbine equator at  $\theta = 90^\circ$ . This is supported by Figure 12, where loads on a portion of the curved blade section above the equator (at  $R/R_{MAX} = 0.82$ ) are shown. The difference in loads at  $\theta = 90^\circ$  is apparently much less in Figure 12 as the depression in interior velocity in Kaman's model is not as severe for blade positions off the equator.

Aside from the obvious difference in load magnitude exhibited by these two models, the frequency content of the time-varying loads is fundamentally different. The single streamtube model predicts basically a two-per-revolution excitation for this operating condition, while the Kaman loads are dominated by four-per-revolution components. This difference is important in determining which vibrational modes are likely to be excited by the aerodynamic loads.

### Summary and Concluding Remarks

Three models designed to predict aerodynamic blade loads for Darrieus Turbines have been compared at two different operating conditions. With regard to flap loading, all three models are in fair agreement with each other at both operating conditions. For lead/lag loading, the single and multiple streamtube models predict similar results. The Kaman model, however, yields substantially lower magnitude with higher frequency content for the lead/lag loads, particularly along the curved blade section.

As none of these models are exact representations of the actual turbine aerodynamics, it is not possible, without some experimental data, to select the most appropriate model. Thus, the 17 m turbine should be designed with appropriate safety factors so the upper and lower bounds of predicted loads may be accommodated. The eventual collection of experimental data on the 17 m turbine should give the best guidance for selecting the most accurate model, so future designs may benefit from more certain load predictions.

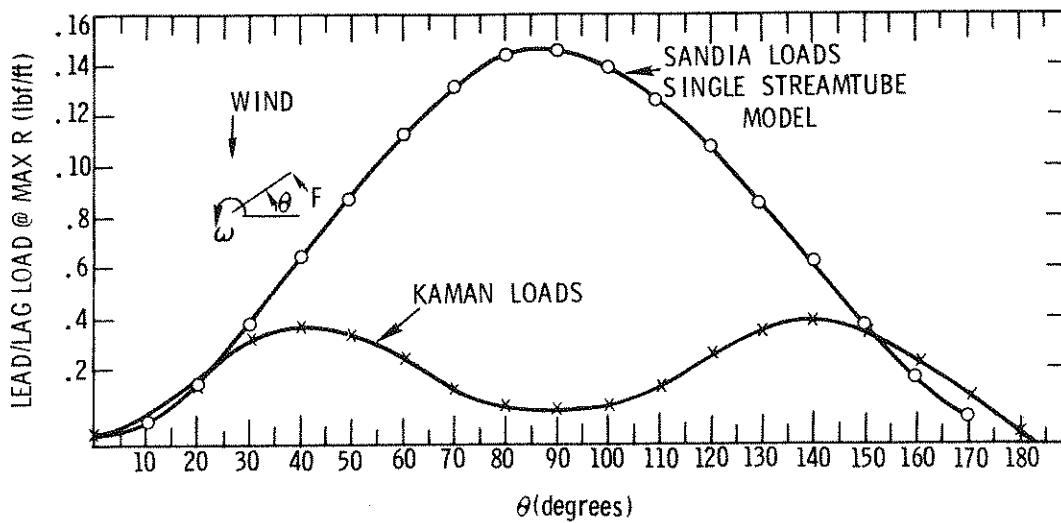


Figure 11. Lead/Lag Load Variations at  $R/R_{MAX} = 0.82$ , 50 RPM, 30 MPH

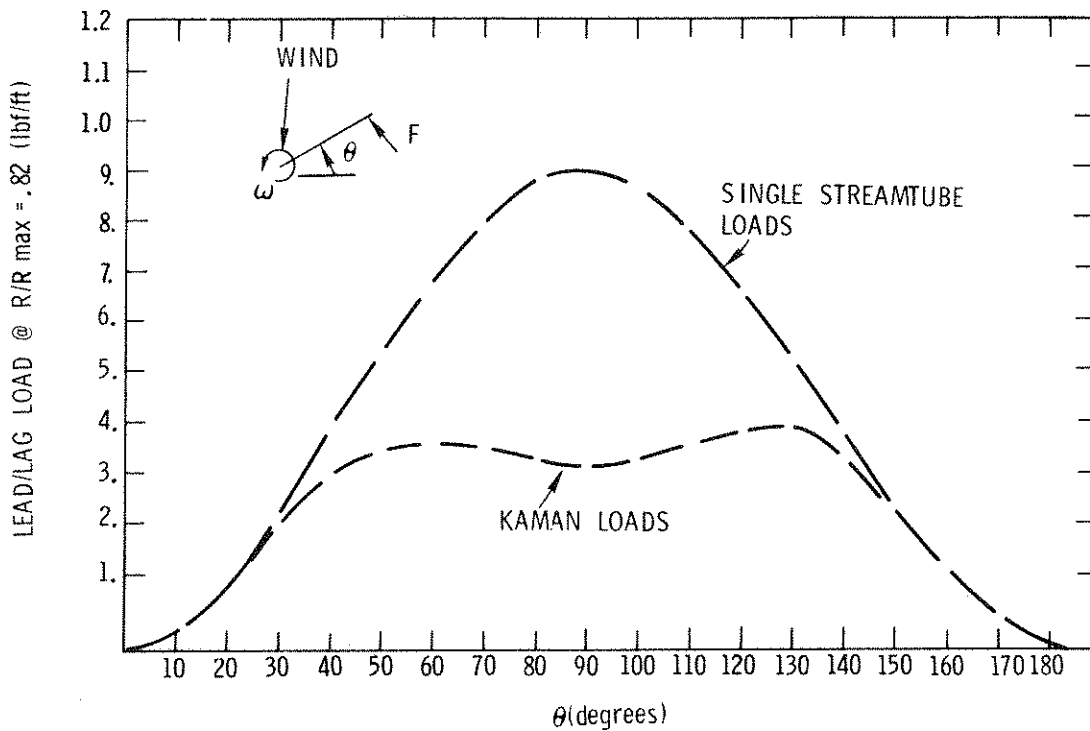


Figure 12. Lead/Lag Load Variations at Turbine - Beltline, 50 RPM, 30 MPH

### 5 Meter Turbine Performance

During the previous two quarters, experimental data on the aerodynamic performance of the 5 m turbine have been collected. This section summarizes the current results of the test program. Utilizing the "method of bins," [2, 8] torque-wind speed characteristics were obtained for the 5 m turbine operating in a two-bladed configuration at rotational speeds of 87.5 rpm, 137.5 rpm, 150 rpm, and 175 rpm. This information was used to deduce the power coefficients

$C_p = P/1/2\rho AV^3$  as a function of the tip speed ratio  $R\omega/V$  and  $K_p = P/1/2\rho A(R\omega)^3$  as a function of the advance ratio  $V/R\omega$ . The results indicate a somewhat poorer performance than expected from comparison with wind tunnel test data for the 2 m turbine. It appears from aerodynamic model calculations that the discrepancy can be explained qualitatively by the poor aerodynamic properties of the straight blade sections on the 5 m turbine.

### Test Setup

Figure 13 shows a component diagram of the 5 m turbine system. The turbine is connected to an induction machine through fixed ratio gears. Nominal rotational speed of the turbine is determined by the synchronous speed of the induction machine and the gear ratio employed. The induction machine can act as either a motor, delivering power to the turbine from the utility line, or a generator, delivering power to the utility line from the turbine.

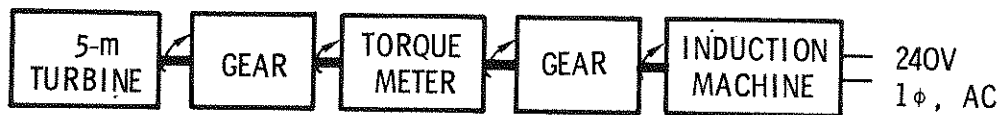


Figure 13. The 5-m Turbine System

Use of an induction machine poses two potential problems: (1) rotational speed is not constant due to the torque-slip characteristic of the machine and (2) torque measurements include the inertial effects of the varying rotational speed. The first problem is not of practical consequence; it has been found that turbine rotational speed varies within about 2 rpm of nominal speed. The second problem is more serious since inertial torques can be substantial in a rapidly changing wind environment. It has been found, however, from model system computations that this effect tends to average out if a sufficiently large number of samples are taken.

Figure 13 implies that the torque meter measures not only the torque due to aerodynamic forces but also friction, in the turbine shaft bearings. Friction torque can represent in some cases a significant fraction of the torque meter reading and must be taken into account to obtain an accurate estimate of turbine performance. A series of tests were performed in which the shaft without the blades was rotated. Weights were attached equal to the weight of the blades. It was found that friction torque decreased slightly with time, presumably due to warmup of the bearing grease.

Wind speed measurements were taken at two locations using cup-type anemometers. The first location was about two turbine diameters in the general up-wind direction from the turbine shaft at a height corresponding to the midpoint of the turbine. The second location was atop the turbine outrigger which necessitated a wind shear correction factor of 0.92 based on referring the measurements to the turbine midpoint by the usual 1/7 power law.

## Data Reduction

A sample strip chart record of torque and wind speed as functions of time is shown in Figure 14. Such records have been hand digitized for input to the data reduction code BINS. This code samples torque and wind speed at a specified constant increment of time using straight-line interpolation between digitized points. All torque samples corresponding to wind speed samples which fall in a given wind speed range (i.e., bin) are averaged. The torque samples are corrected by adding a value of friction torque to obtain the turbine shaft torque due to aerodynamic forces. A wind speed distribution is derived by dividing the number of samples in each bin by the total number of samples. Figures 15 through 22 show the wind speed frequency distribution and torque as functions of wind speed. Note that each of these figures is derived from data collected on several days which accounts for the multimodal shapes of the wind speed frequency distributions. Torques corresponding to low values of wind speed frequency should be considered suspect since the torque average is based on relatively few samples.

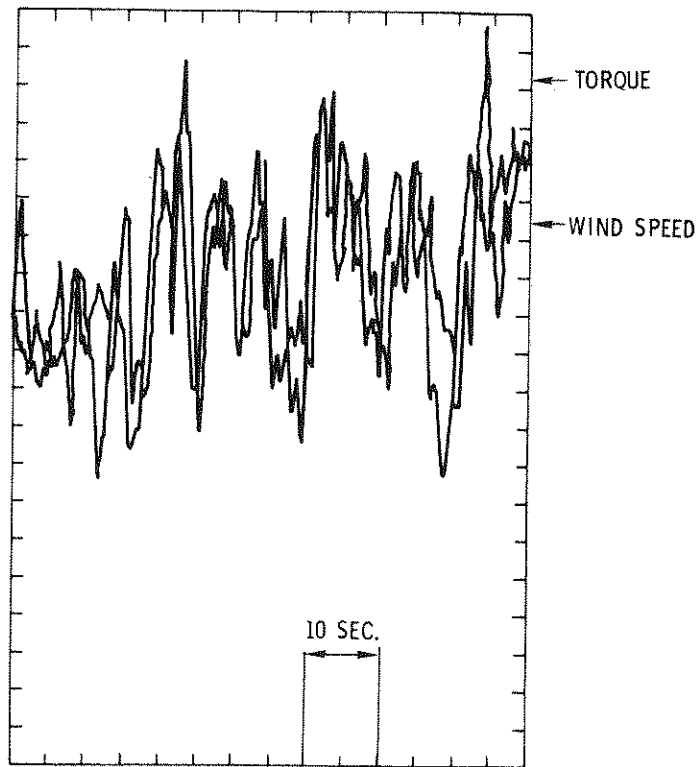


Figure 14. Sample Record of Torque and Wind Speed

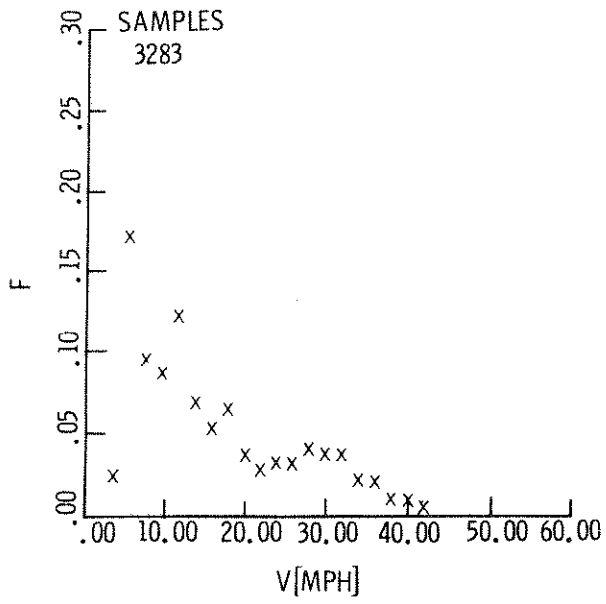


Figure 15. Wind Speed Frequency Distribution, 87.5 RPM

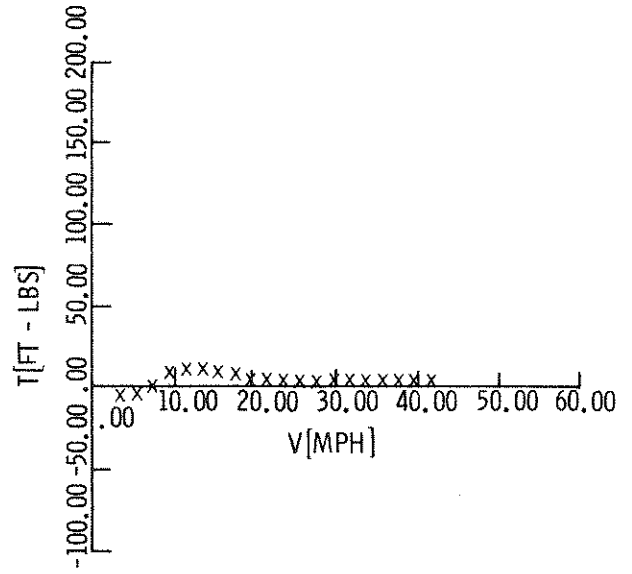


Figure 16. Average Torque, 87.5 RPM

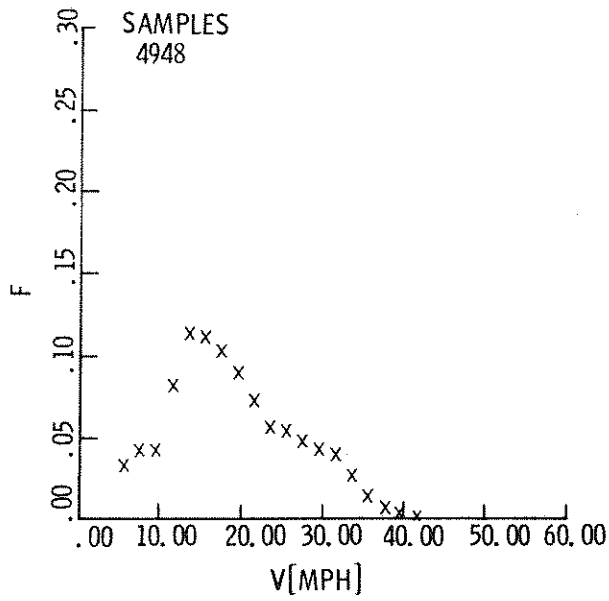


Figure 17. Wind Speed Frequency Distribution, 137.5 RPM

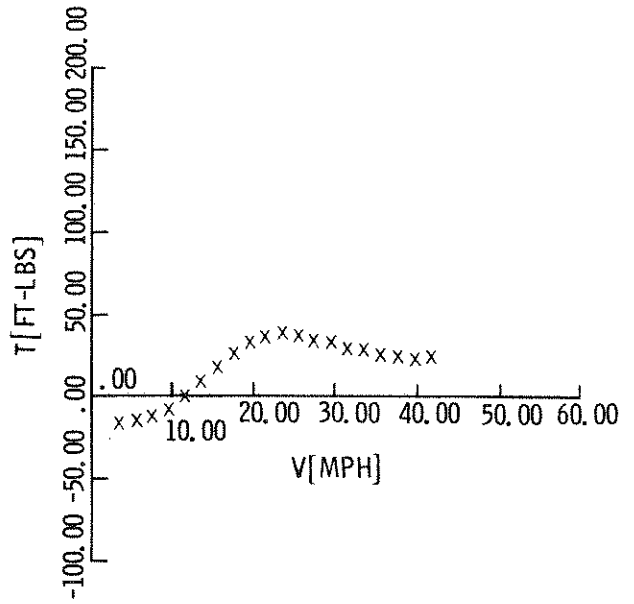


Figure 18. Average Torque, 137.5 RPM

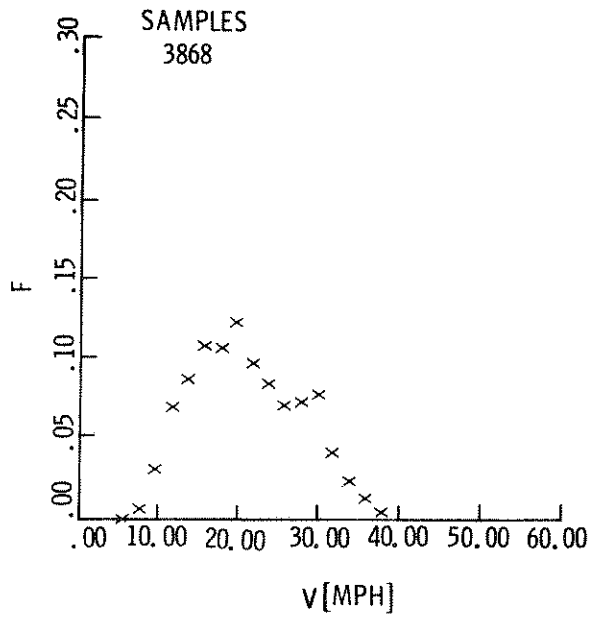


Figure 19. Wind Speed Frequency Distribution, 150 RPM

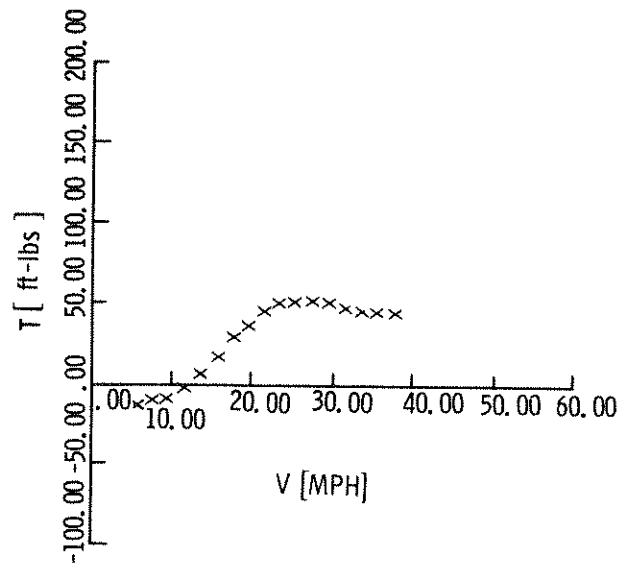


Figure 20. Average Torque, 150 RPM

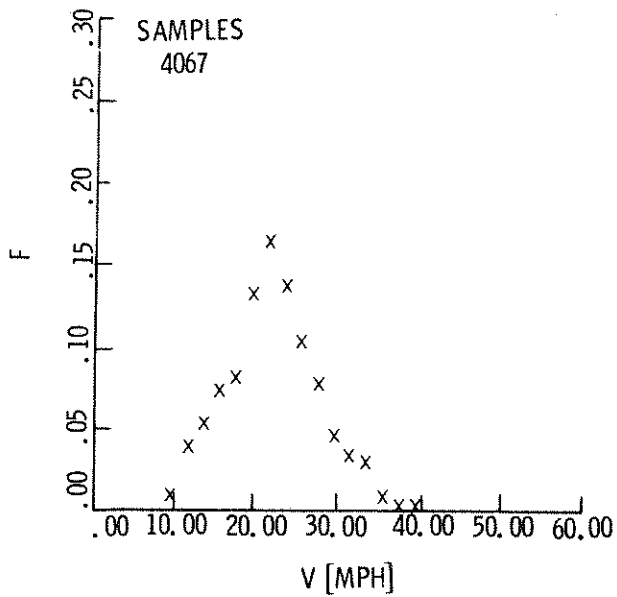


Figure 21. Wind Speed Frequency Distribution, 175 RPM

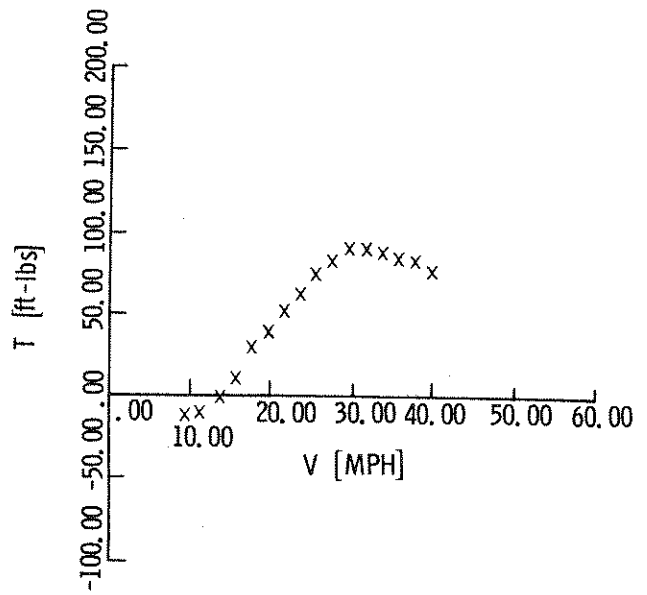


Figure 22. Average Torque, 175 RPM

## Power Coefficients

The information in Figures 15 through 22 can be used to deduce the power coefficients  $C_p = P/1/2\rho A(R\omega)^3$  as a function of the tip speed ratio  $R\omega/V$  and  $K = P/1/2\rho A(R\omega)^3$  as a function of the advance ratio  $V/R\omega$ . Figures 23 through 30 show the power coefficient characteristics as functions of the Reynolds number,  $Re$ , which is based on the turbine tip speed  $R\omega$  and the blade chord  $c$ . The power coefficient  $K_p$  is presented for three reasons: (1)  $K_p$  shows that power reaches a maximum with respect to wind speed when the turbine rotational speed is constant, (2)  $K_p$  is a more useful characteristic of turbine performance for turbines operating in the synchronous mode and (3) large errors in tip speed ratio can occur due to errors in measuring the wind speed.

The 5 m turbine appears to have poorer performance than expected. This is based on extrapolation of wind tunnel test data for the 2 m turbine [2, 9]. For example, maximum power coefficient  $C_{p_{max}}$  for the 5 m turbine operating 175 rpm was found to be about 0.2, while wind tunnel test results indicate that  $C_{p_{max}}$  should exceed 0.3. Calculations have been performed with the multiple-streamtube aerodynamic model in an attempt to understand the decrease performance. One difference between the two turbines is that the straight blades on the 5 m turbine consisting of roll-formed sections are of poor and unknown aerodynamic quality while the 2 m turbine consists entirely of blades of NACA 0012 crosssection.

Aerodynamic characteristics of the straight blade were assumed to be those of a flat plate. The specific geometry consisted of a thickness that was nine percent of the chord, cylindrical leading edge, and a sharp trailing edge like a wedge with an included angle of  $6^\circ$ . The minimum drag coefficient for this section is 0.04, which is about five times that of the NACA 0012, and has an axial force coefficient which is negative for angles of attack less than  $90^\circ$ . Figure 31 presents the calculations for this flat plate airfoil. The curve labeled "low drag" uses NACA 0012 data for the straight section and the curve labeled "high drag" uses the flat plate data. The computed peak power coefficient is reduced from 0.38 to 0.28. Inclusion of wind shear reduces the peak power coefficient even further to 0.26. This is still above the measured value of 0.2. The current computer model is not valid in an absolute sense, rather it tends to overpredict. The model calculations, however, give a good qualitative explanation of the 5 m performance. The effect of the straight blade aerodynamics appear to be more significant than was previously thought.

Another factor contributing to the poor performance is the condition of the curved blades. Numerous pimple-like blemishes were found on the fiberglass skin. One blade showed evidence of a delamination which resulted in a considerable change in the airfoil crosssection. In particular, the section was no longer symmetrical.

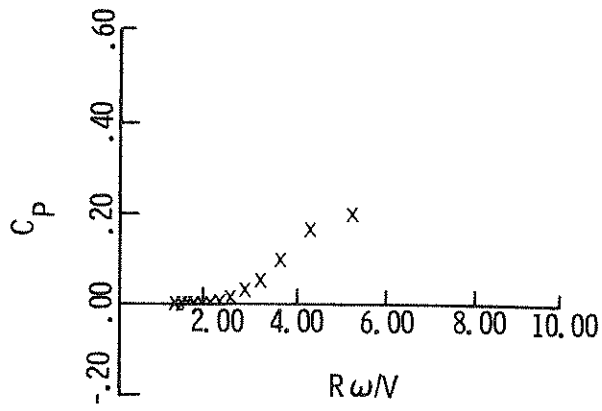


Figure 23. Power Coefficient  $C_p$  ( $Re = 2.6 \times 10^5$ )

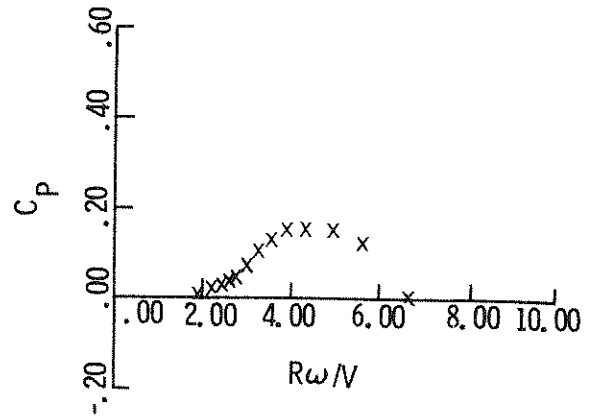


Figure 24. Power Coefficient  $C_p$  ( $Re = 4.0 \times 10^5$ )

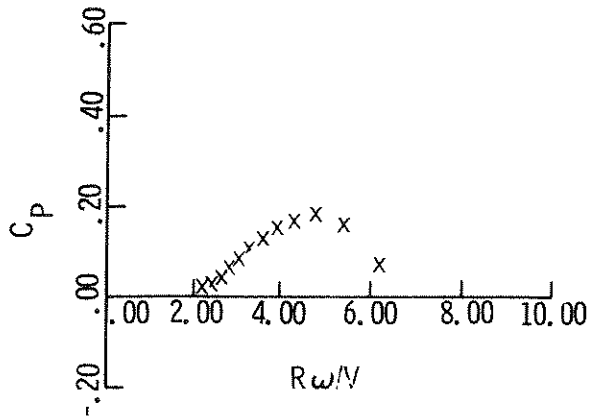


Figure 25. Power Coefficient  $C_p$  ( $Re = 4.4 \times 10^5$ )

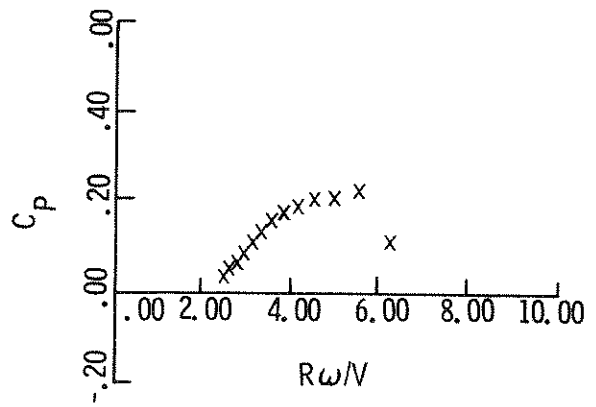


Figure 26. Power Coefficient  $C_p$  ( $Re = 5.1 \times 10^5$ )

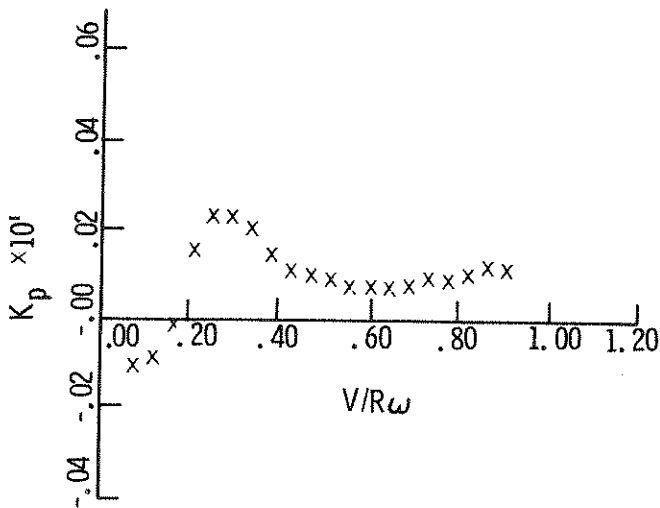


Figure 27. Power Coefficient  $K_p$  ( $Re = 2.6 \times 10^5$ )

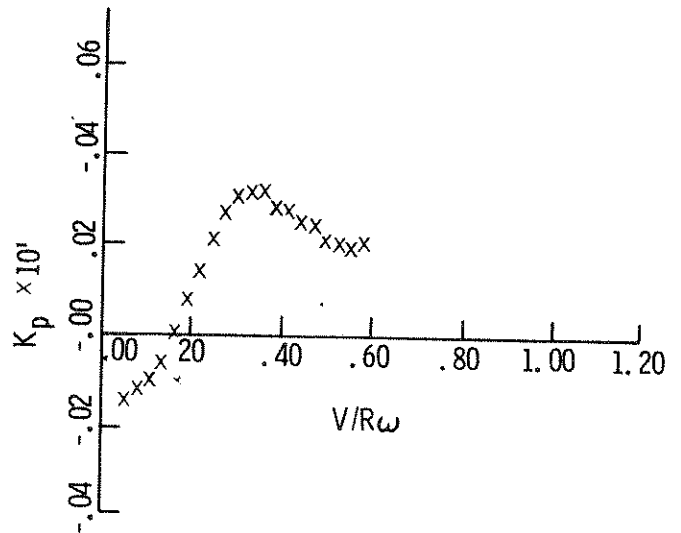


Figure 28. Power Coefficient  $K_p$  ( $Re = 4.0 \times 10^5$ )

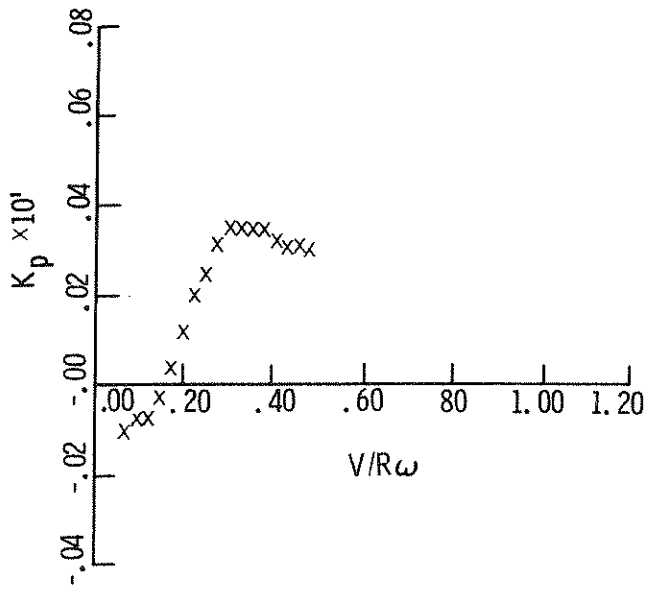


Figure 29. Power Coefficient  $K_p$  ( $Re = 4.4 \times 10^5$ )

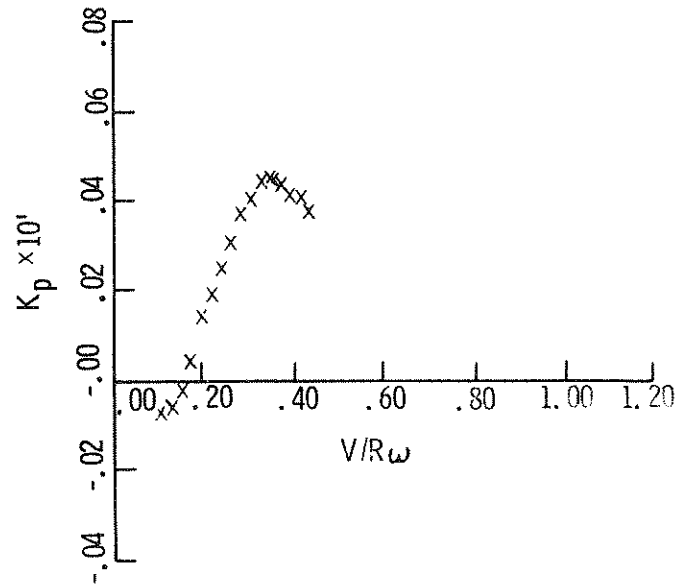


Figure 30. Power Coefficient  $K_p$  ( $Re = 5.1 \times 10^5$ )

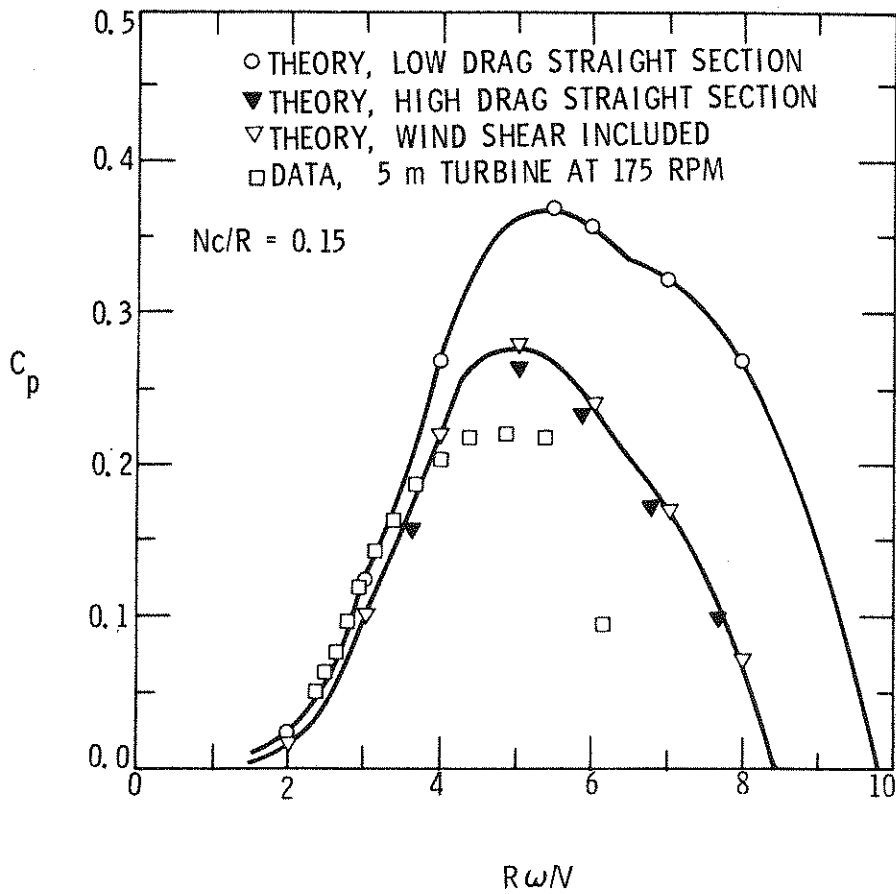


Figure 31. Comparison of Theory and Data for 5 m Turbine at 175 RPM

### III. ELECTRICAL SYSTEMS AUTOMATIC CONTROL AND DATA ACQUISITION

The goal of automatic control and data acquisition for the wind turbine program is to reduce manpower costs of operation by having cost effective automation capable of operating and monitoring the wind turbine system independently of on-site personnel. To achieve this goal Sandia Laboratories' Wind Turbine Test Facility is equipped with a microprocessor system and peripheral electronic devices which interface the processor with the turbine's power systems, operating sensors, anemometers, and output recording devices. The microprocessor is a recent development in solid state electronics which enables a miniature but complete digital computer to be built in the form of integrated circuits in a very small, inexpensive package.

The equipment in the test facility consists of a TI Silent 700 teleprinter, a set of control and instrumentation racks, and a power control console. The microprocessor based automation is achieved with a paper tape punch, reader, an Intel Intellec-80 microcomputer, and an ICOM dual floppy disk magnetic data storage system. Signal conditioning is performed by a DORIC 100-channel analog-to-digital converter. The power control console contains all operating controls and instrumentation for the 5-hp induction machine to operate the 5-meter VAWT.

Figure 32 is a simplified block diagram of a microprocessor system for automatic control of the VAWT. In essence the microprocessor is an automatic operator which runs the start motor, generator, or brakes as a function of the wind conditions and the state of the VAWT.

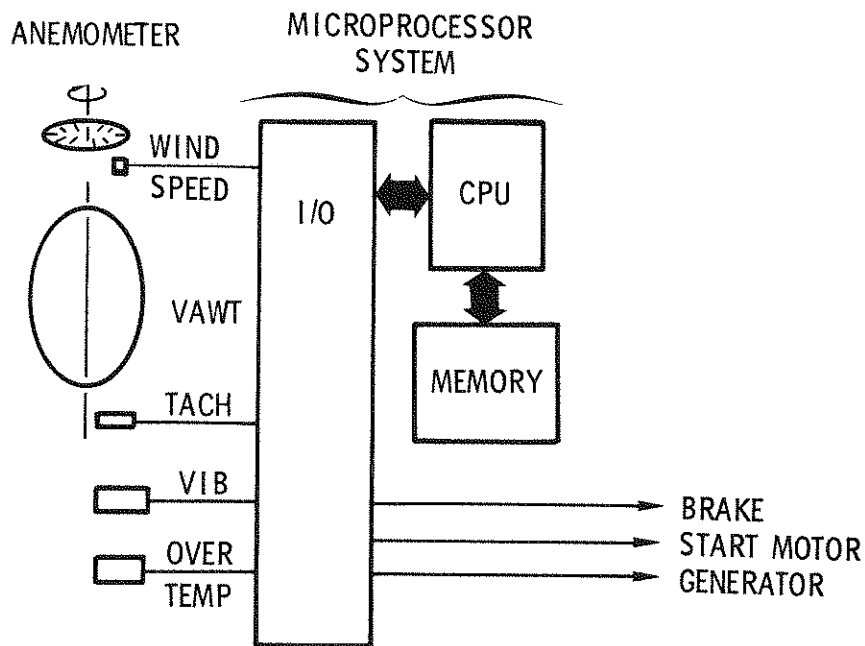


Figure 32. Automatic Control of VAWT

Figure 33 shows a simplified program flowchart for the microprocessor VAWT control. The advantage of this approach is that the operation is governed by software written into a programmable read only memory (PROM) which can be programmed to carry out all the required measurements and performance checks to ensure safe, reliable, and efficient operation of the wind turbine. Changes to the program can be made simply by erasing the PROM and reprogramming it.

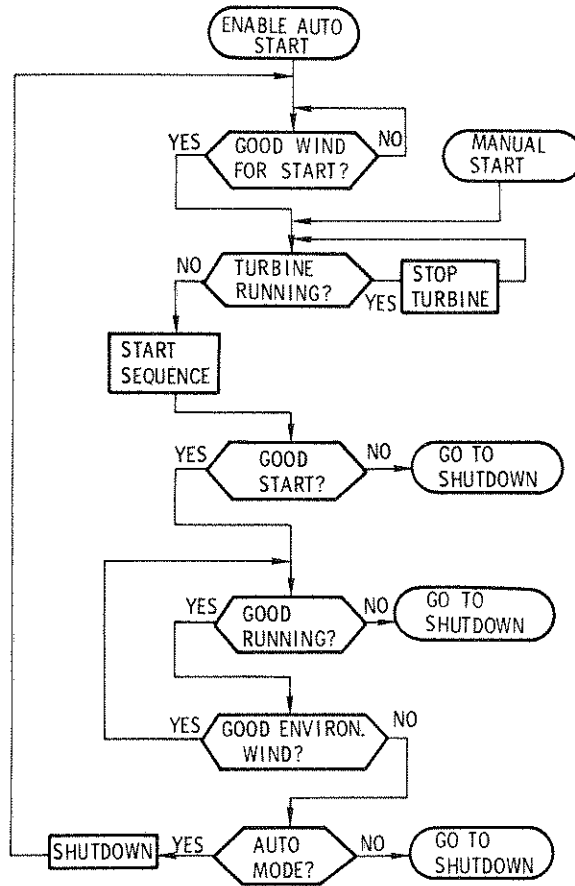


Figure 33. Microprocessor Program Flowchart for VAWT

Basically, the program shown in Figure 33 determines when to run the VAWT based on wind speed history. If sufficient wind speed is observed for a sufficient time then the turbine is started. If the wind's speed falls below an acceptable level for more than a prescribed time the turbine is shut down. Both wind speed and time criteria for running are programmable and different values may be chosen depending on the site and particular turbine characteristics. Once the turbine is running the microprocessor monitors sensors such as bearing and generator temperature structural vibration, turbine shaft speed, and electrical power. If an unusual condition is observed the system will notify responsible personnel. If a malfunction occurs, the system will execute an

orderly shutdown. A microprocessor wind turbine controller which displays the above functions was demonstrated on May 17-20, 1976, at the vertical Axis Wind Turbine Technology Workshop.

Figure 34 displays block diagrams of wind instrumentation systems based on the conventional manual method and an automated data acquisition approach. In the manual approach the anemometer and wind turbine torque data are stored on a strip chart recorder. The chart is then digitized and the data is stored on magnetic tape for input to a computer for data processing and output plotting. This approach has a number of severe drawbacks. First, the strip chart recording is not appropriate for taking accurate data over extended periods of time. The amount of chart paper required for long runs is enormous and the accuracy obtained is inversely related to the paper's speed because of ink smear and noise. Once the long lengths of recordings are made the information must be digitized for computer processing. This procedure requires extensive, time consuming, manual labor.

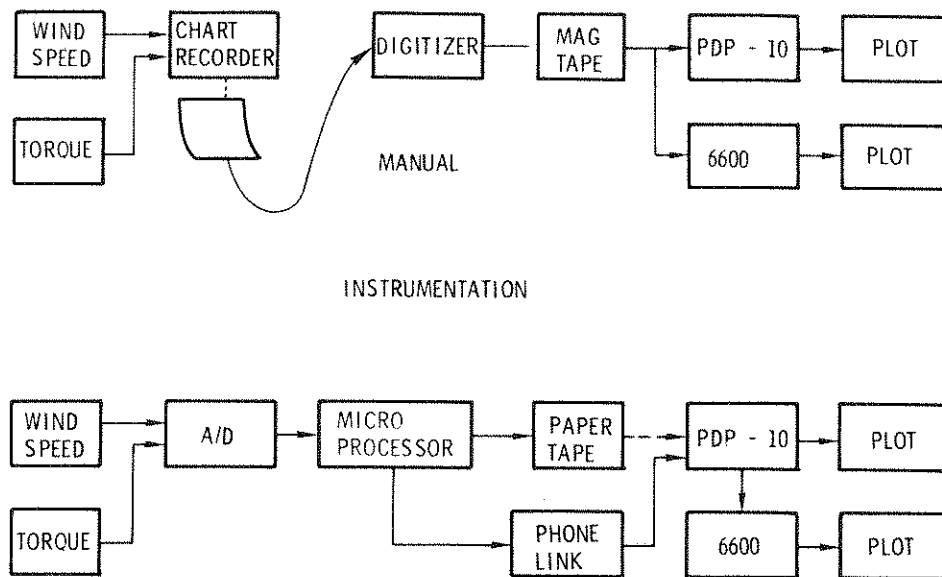


Figure 34. Block Diagrams of Wind Instrumentation Systems

The automated approach alleviates the above problems by performing the answer to digital (A/D) conversion directly from the test instruments. The digital data is processed by a microprocessor and recorded onto a paper tape, magnetic cassette and fed directly to a large computer via a phone link. A further step may be taken by using digital instruments to eliminate the A/D converter entirely.

## IV. STRUCTURES

### Modal Analysis

Further work on the selection of the dominant modes of the VAWT has been done. In addition to the previously reported norm used in the selection procedure for the dominant modes, new norms which measure the contribution of the individual modes to the overall system's kinetic, potential, and total energy have been derived and programmed. Actual modal ordering will be completed once the loads analysis becomes available.

For check out of the procedures for calculating the modal participation norms, loads were obtained for the blades under the conditions for 60 mph wind at a rotational speed of 45.4 rpm. Loads for the struts were obtained from the loads on the straight sections of the blades using appropriate symmetry conditions. Mode shapes and frequencies for the VAWT to use with the loads were obtained at zero rpm because a nonlinear analysis at 45.5 rpm was not available to use to obtain initial tensions in the blades and struts due to centrifugal forces.

The results of the participating modal norm analysis showed that by far the most energy absorbing mode is the first chord-wise mode at 3.182 Hz. The mode ranked first with each norm and its ranking is not expected to change when initial tensions are applied to the blades. The next important mode is flatwise motion of the straight sections of the blades. However, the results are questionable because initial tension will change the results.

### Blade Buckling Studies, 17 Meter

A buckling analysis of the 17 m wind turbine blade has been initiated. It is assumed that the worst condition is in the parked condition and is due to aerodynamic loads. The blade analyzed is upwind of the tower.

Two methods to study the buckling behavior are being used in parallel. The first uses the general purpose finite element code which has been described in previous Technical Quarterly Reports. This includes all large displacement effects. The second method is a closed-form approach using Castigliano's theorem. It also considers the straight-sections and the struts to behave as beam-columns. Both methods assume material linearity.

Though there are no definitive results at the moment, there are indications that if there are problems, they will occur in either the straight or strut sections of the blade.

### Suggested Method for Establishing Fatigue Life of 17 Meter VAWT Blades

The material used to carry loads in the 17 m VAWT blades is extruded aluminum 6061-T6. Little data exists on the fatigue properties of 6061-T6 for varying amounts of mean and alternating stress. However, with the aid of MIL-HDBK-5B, [10] a good approximation for its behavior can be obtained.

Page 3-185 of MIL-HDBK-5B contains a figure depicting a constant-life diagram for the fatigue behavior of unnotched wrought 6061-T6 aluminum alloy. The ultimate tensile strength of this alloy is 44,300 psi as opposed to 38,000 psi for extruded 6061-T6. From the referenced figure, Table III can be constructed. This table gives fatigue strength versus number of cycles at zero mean stress.

TABLE III  
Unnotched Wrought 6061-T6

<u>Fatigue Strength (psi)</u>	<u>N (No. of Cycles)</u>
32700	$10^4$
24200	$10^5$
18800	$10^6$
13900	$10^7$

Using this table and the ultimate strength (1 cycle), a S-N diagram can be drawn, Figure 35. Wrought 6061-T6 is the upper curve in this figure.

The curve for extruded 6061-T6 is obtained in the following manner. The operational limit for infinite life ( $10^7$  cycles) of 6,000 psi is assumed. This is based on Kaman Aerospace rotor experience with initially unnotched extruded 6061-T6. The effect of notches and holes is apparently included in this experience factor. The lower limit (1 cycle) is equal to the ultimate strength of extruded 6061-T6. Using these end points and the fact that the shape of the S-N curve for extruded 6061-T6 should be the same as the unnotched wrought 6061-T6, the lower curve in Figure 35 can be drawn. Also used is the fact that the curve slope should approach zero at infinite cycles. Table IV can now be constructed from this curve. Also included in Table IV are data received via personal communication from Kaman on the fatigue strength obtained using a similar method. Since the data received from Kaman (second column, Table II) is always less than the data obtained from the Sandia curve, it is suggested that the Kaman data be subsequently used in order to obtain a lower limit on fatigue life.

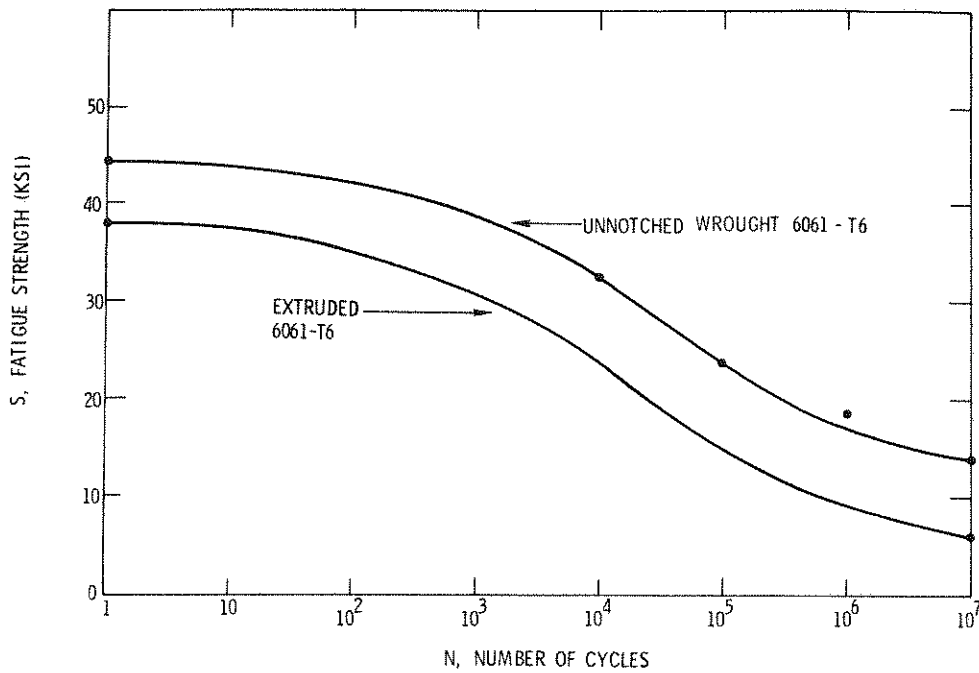


Figure 35. Fatigue Strength vs Number of Cycles

TABLE IV

Extruded 6061-T6

Fatigue Strength (psi) Sandia Curve	Fatigue Strength (psi) Kaman Curve	N (No. of Cycles)
30500	29000	10 <sup>3</sup>
23700	22600	10 <sup>4</sup>
14900	14200	10 <sup>5</sup>
9100	8600	10 <sup>6</sup>
6000	6000	10 <sup>7</sup>

A Goodman diagram [11] is now constructed using the data from Table II. This diagram, shown in Figure 36, relates an allowable alternating stress versus mean stress for a specified life (number of cycles). For each specified number of cycles a straight line is drawn from the allowable alternating stress at zero mean stress to the ultimate tensile strength (zero alternating stress). In reality this line is curved (same end points) with the data lying above the straight line. A commonly used curved line which lies close to test data is the Gerber line. However, use of the Gerber line results in a less conservative design, and it is suggested that it not be used in 17 m VAWT blade design.

It should be noted at this time that 10<sup>7</sup> cycles translates into about 3,300 hours at 50 rpm (1 stress cycle per revolution). Hopefully the turbine blades are expected to last 20 years of operation, and 3,300 hours is but a small portion. The curve in Figure 36 labeled 10<sup>7</sup> cycles can be

replaced by an identical curve labeled by a significantly higher number (i.e.,  $10^9$  cycles). This is due to the fact that for most engineering materials, aluminum included, a S-N curve, such as that shown in Figure 35, is quite flat for cycles greater than  $10^7$ .

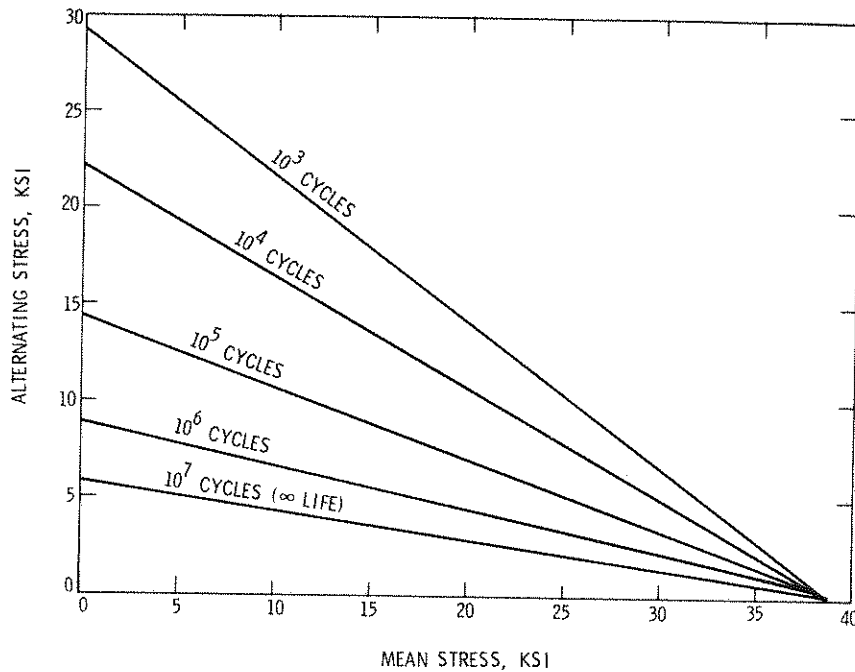


Figure 36. Goodman Diagram, Extruded 6061-T6

The curves in Figure 36 should be used to predict fatigue life during turbine operation utilizing a cumulative damage theory. The simplest of these theories and also the one which is commonly used by helicopter rotor manufacturer's [12] has been denoted as Miner's Cumulative Damage Theory. [13] Reference 3 states this theory:

All applied cycles of stress above an endurance limit produce fatigue damage. Furthermore, the fractional life reduction is calculable as the summation of ratios of applied cycles ( $n_i$ ) to fatigue life ( $N_i$ ) provided each ratio is obtained at the same cyclic and steady-stress amplitudes. The fatigue life is defined as the amount of time required for the sum of these damage ratios to equal unity.

Mathematically, this states that fatigue life is "used up" when:

$$\sum_i \frac{n_i}{N_i} = 1$$

For example, using Figure 36, a blade which sees a mean stress of 12,000 psi and an alternating stress of 10,000 psi has a life time ( $N_i$ ) of  $10^5$  cycles. If during its proposed operational life it actually sees  $10^3$  cycles ( $n_i$ ) at this condition it uses up  $(n_i/N_i) = 0.01$  of its fatigue life. It has not been clearly shown in the literature whether Miner's relation yields conservative results.

Reference 14 indicates that there is available data which indicates that the right-hand side of the above equation can vary from 0.3 to 3.0. This depends on a number of items, including material type, number of load levels, initial application of high and low stress, and randomness of the load. It is suggested that a value of unity be used for initial studies on the fatigue life of the 17 m VAWT blades for the following reasons:

1. It is a median value and easy to apply.
2. There is no present conclusive evidence that another number is better.
3. It is widely used in the helicopter rotor field.

It has been suggested that the 17 m VAWT blade fatigue life be estimated using Miner's relation and a Goodman diagram determined from an S-N curve which is based on data in MIL-HDBK-5B and data obtained from Kaman.

#### Turbine Base/Tower/Tiedown Components

A static structural analysis of the 17 m base/tower/tiedown system was completed this quarter. The detailed design is shown in Figure 37, and a schematic of the finite element model used for structural analysis is shown in Figure 38. The SAP IV linear, finite element structural code was used for the analytical results given here.

The major loads acting on the tower are shown in Figure 38 as  $F_1$  and  $F_2$ . These loads are due to unbalanced aerodynamic forces acting on the turbine blade during rotation. Two specific load cases have been considered. The first is a "design" load ( $F_1 = 9000$  lbs;  $F_2 = 3000$  lbs). These loads correspond approximately to a 75 rpm, 80 mph runaway condition. The second ( $F_1 = 5000$  lbs,  $F_2 = 1500$  lbs) is a maximum "normal operating" load, corresponding to 52.5 rpm with 60 mph winds.

The aerodynamic tower resultants tend to vary as the turbine rotates, which suggests that a dynamic analysis may be more appropriate for the tower components. It is felt, however, that the high natural frequencies of the tower/ base/tiedown components, relative to the aerodynamic load frequencies, make the static results meaningful, for engineering design purposes. A normal mode dynamic analysis for the complete turbine is currently being pursued and the legitimacy of using a static analysis will be checked pending completion of the dynamic analysis.

The transverse loads  $F_1$  and  $F_2$  dominate the response of the tower and tiedown components. In analyzing the base structure, two additional loads must be considered. These are the brake torque reaction load (50,000 ft-lbs) and the net axial load due to turbine weight and tiedown thrust (approx. 35,000 lbs). Both of these loads act at the vertex of the base.

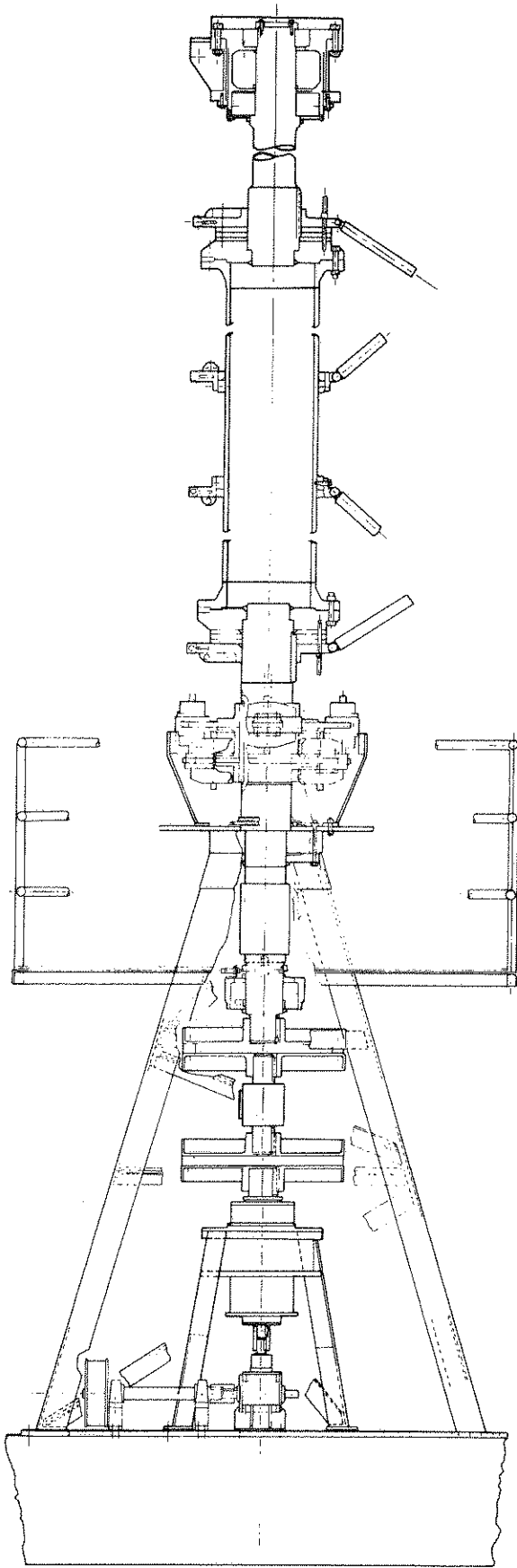


Figure 37. Details of Turbine Base and Tower

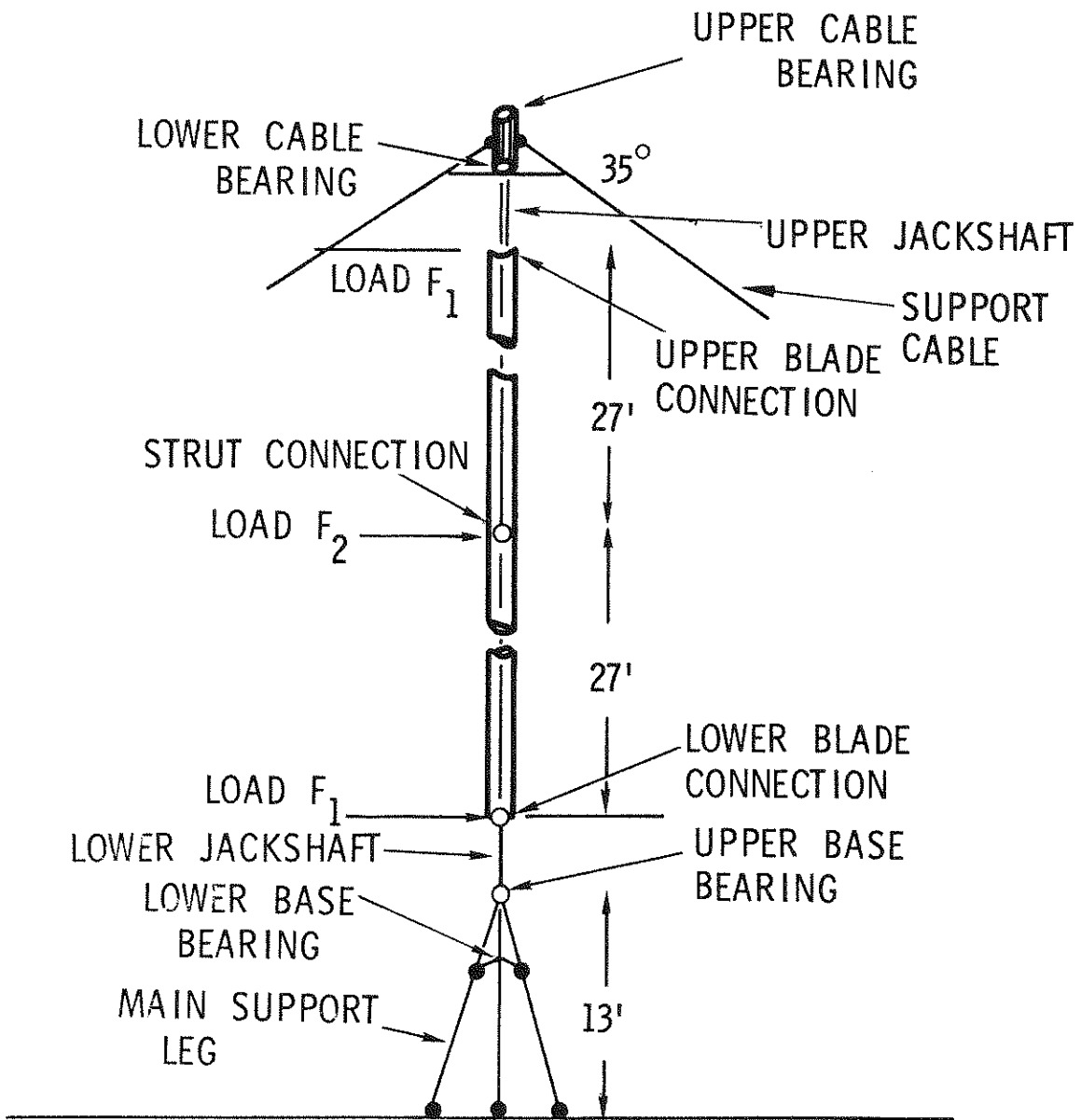


Figure 38. Finite Element Model of Base/Tower/Tiedown System, 17 m Turbine

Table V summarizes the response of the tower and tiedown to the transverse aerodynamic loading. A cable pretension of 6,000 lb was used in these calculations. It is clear that at the design load condition, this pretension is not adequate as the downwind cable is nearly slack. A cable pretension between 8,000 and 12,000 lb will be used in the field to avoid this condition\*.

TABLE V  
Load and Deflection Data - Tower and Bearings

	<u>Design Load</u> <u>(75 rpm 80 mph)</u>	<u>Normal Operating</u> <u>(52.5 rpm 60 mph)</u>
Max. Tower Deflection	1.2 in @ Strut Connection	0.67 in @ Strut Connection
Cable Tension, Preload of 6,000 lb	11,800 lb (upwind) 200 lb (downwind)	9,200 lb (upwind) 2,800 lb (downwind)
Lower Cable Bearing Side Load	2,798 lb	1,533 lb
Upper Cable Bearing Side Load	6,756 lb	3,703 lb
Cable Bearing Thrust Load	13,766 lb	13,766 lb
Lower Base Bearing Side Load	9,938 lb	5,358 lb
Upper Base Bearing Side Load	21,388 lb	11,622 lb
Base Bearing Thrust Load	13,766 lb + Turbine Weight	13,766 lb + Turbine Weight
Max. Tower Bending Moment	951,500 in-lb @ Strut Connection	499,300 in-lb @ Strut Connection
Max. Tower Bending Stress	3,524 PSI	1,849 PSI
Max. Lower Jackshaft Bending Moment	405,100 in-lb @ Upper Base Bearing	218,400 in-lb @ Upper Base Bearing
Max. Lower Jackshaft Bending Stress	5,660 PSI	3,051 PSI
Max. Upper Jackshaft Bending Moment	768,700 in-lb @ Upper Blade Connection	421,300 in-lb @ Upper Blade Connection
Max. Upper Jackshaft Bending Stress	10,740 PSI	5,886 PSI

\*Preliminary calculations indicate that the increased axial load caused by the additional cable tension can be adequately handled by the thrust bearing and base as currently designed.

All stresses in the tower are apparently a small fraction of the yield strength of the mild steel used for these components. The most highly stressed component appears to be the upper jackshaft, where bending stresses of 10,740 psi occur under design loads.

An analysis of the main base structure indicates that the torque applied at the base vertex from the brake produces the largest bending moments in the base elements. In particular, a stress of 22,000 psi may be realized in the main support legs at the vertex due to brake twisting. This stress is believed to be conservatively high, as the actual design has gussets at the vertex which are not included in the model.

In conclusion, the base/tower/tiedown system as it is now designed can readily withstand the static loads imposed by the turbine blades. To avoid slack in the downwind cable, the cable tension should be between 8,000 to 12,000 lb.

#### Turbine Tie-Down, 17 Meter

There are two principle aspects, or phases, to the design of a cable, tiedown system for the vertical axis wind turbine. The first is that of establishing geometric, physical and mechanical properties of the system for adequate load carrying capability and tower stiffening. Important properties include the number of cables, the cable elevation angle, cable density, active cable area and cable stiffness. The second aspect of the design is that of determining initial cable tension and sag to insure sufficient blade clearance and load retention after tower deflection. These two aspects of design are actually coupled together due to the dependence of cable stiffness on initial tension. The dependence is nonlinear and therefore difficult to handle, especially when the nonlinearities become large. With proper selection of cable properties and initial tensions the nonlinear effects can be minimized, thus permitting independent treatment of the two phases. This approach will be used here.

#### Phase I Design Results

Symmetrically distributed numbers of cables have a significant erection advantage over odd, or unsymmetrically distributed numbers of cables. This is because even numbers of cables can be mounted and tensioned in pairs rather than all at once. Four cables, at equally spaced azimuth positions, were selected for the 17 meter, VAWT tower tie-down. Two cables offer stiffness in only one vertical plane, and six cables were judged to be too many for cost reasons.

The cable elevation angle was selected as that which gave a maximum horizontal stiffening effect to the blade support tower and a minimum bending moment at the base of the tower. This angle is  $35^{\circ}$  measured from a horizontal plane.

Cable "outriggers" at the top of the tower were eliminated because of relatively small stiffening effects, undesirable translation-rotation coupling at the top of the tower and added costs. They were not needed to reduce the blade-cable strike probability because of the relatively shallow cable elevation angle of  $35^\circ$ .

A minimum cable-tower horizontal stiffness at the top of the tower of approximately 9,000 lb/in was established for the four-cable tie-down system. This resulted in approximately a one inch, downwind, horizontal deflection at the top of the tower in an 80 mph wind. (This is the maximum wind speed in which the turbine will be permitted to operate.) In order to meet this stiffness requirement, the following wire rope was selected.

Name and Construction: galvanized bridge strand, 7 strand  
 Linear Weight: 2.07 lb/ft  
 Active Cross Sectional Area: 0.596 in  
 Effective Elastic Modulus:  $25.0 \times 10^6$  psi  
 Breaking Strength: 122,000 lb

Phase II Design, Initial Tension

Because of the nonlinear coupling of cable geometry (sag) and mechanical properties with cable tension, it is possible for results of this phase to effect preliminary design. This design feedback can be eliminated, if cable tension is high enough to minimize nonlinear effects, as will be demonstrated.

There are several features of the cable tension-sag problem which are worth discussing separately. The first is the relationship between tension and midpoint sag in a cable which connects two fixed points in space. These two points are the top of the undeflected blade support tower and the ground connection, see Figure 39.

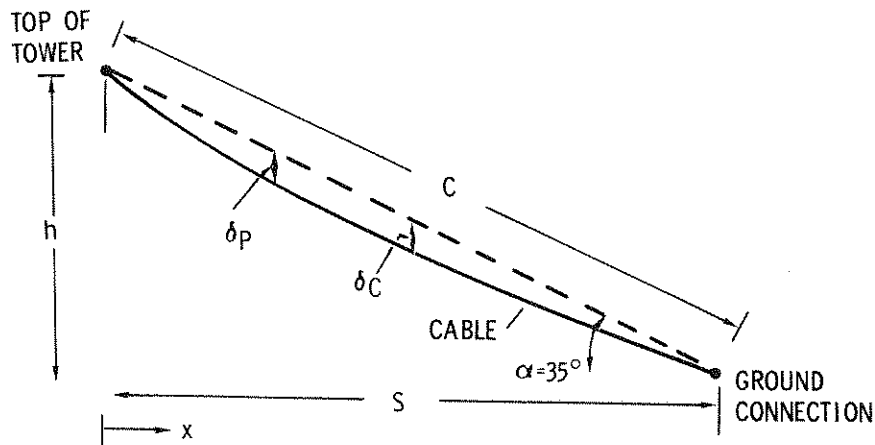


Figure 39. Cable Geometry

The midpoint sag in the cable is given by the parabolic approximation [15]

$$\delta_c = \frac{wc^2}{8T} \cos \alpha \quad (1)$$

where  $\alpha$  is the elevation angle of the undeflected cable, T is the chordwise component of the cable tension (directed along a line connecting the cable endpoints), c is the chord length and w is the linear weight of the cable.

Another feature of the cable tension-sag problem which is of interest is the relationship between cable midpoint sag and sag at some other point. This relationship is

$$\delta_x = \frac{4\delta_c x(s-x)}{C^2 \cos^2 \alpha}$$

where x is measured as shown in Figure 39. For the cable selected for tie-down of the 17 meter turbine, midpoint sag and sag at the point closest to the passing blade are shown in Figure 40. The point on a blade which comes closest to a sagging tie-down cable lies approximately at the intersection of the straight, circular arc and strut blade sections.

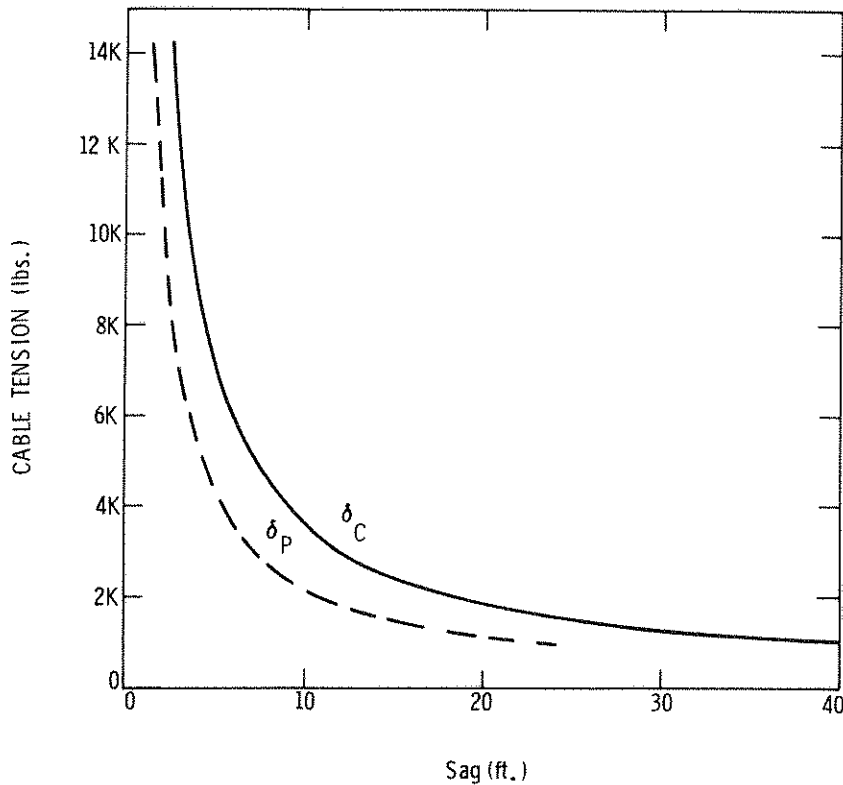


Figure 40. Initial Tension vs Sag

The next question which arises is what happens to the tension and sag in a cable when there is relative motion between the two end points. The relative motion between the end points will be permitted by keeping the ground connection fixed and allowing horizontal motion,  $\Delta c_h$ , at the top of the tower in the plane of the deflected cable. When this motion occurs, part of it is due to elastic stretch (or contraction) in the cable, and part is due to a change in the cable geometry (sag). See Reference 15 for a more complete discussion. The change in chord length,  $\Delta c$ , is related to the change in cable tension,  $\Delta T$ , by

$$\Delta c = \Delta c_h \cos \alpha = \left[ \frac{c \Delta T}{AE} + \frac{\omega^2 c^3 \cos^2 \alpha}{24 (1+b)} \frac{\Delta T (\Delta T + 2T_i)}{T_i^2 (\Delta T + T_i)^2} \right] \quad (3)$$

Numerical results of (3) are presented in Figure 41 for the 17 meter turbine tie-down cable where cable tension change,  $\Delta T$ , is shown as a function of cable chord length change,  $\Delta c$ , and horizontal deflection,  $\Delta c_h$ . Also shown is the 9000 lb/in linear cable stiffness,  $K_s$ , used in the composite tower, tie-down analysis. As indicated in the figure, nonlinear effects become increasingly larger with deflection. Also evident is that the higher the initial cable tension, the greater the permissible deflection before nonlinear effects become strong. From the figure, cables with initial tensions of 12K lbs or greater behave in a nearly linear fashion for horizontal deflections,  $\Delta c_h$ , up to about 1 inch.

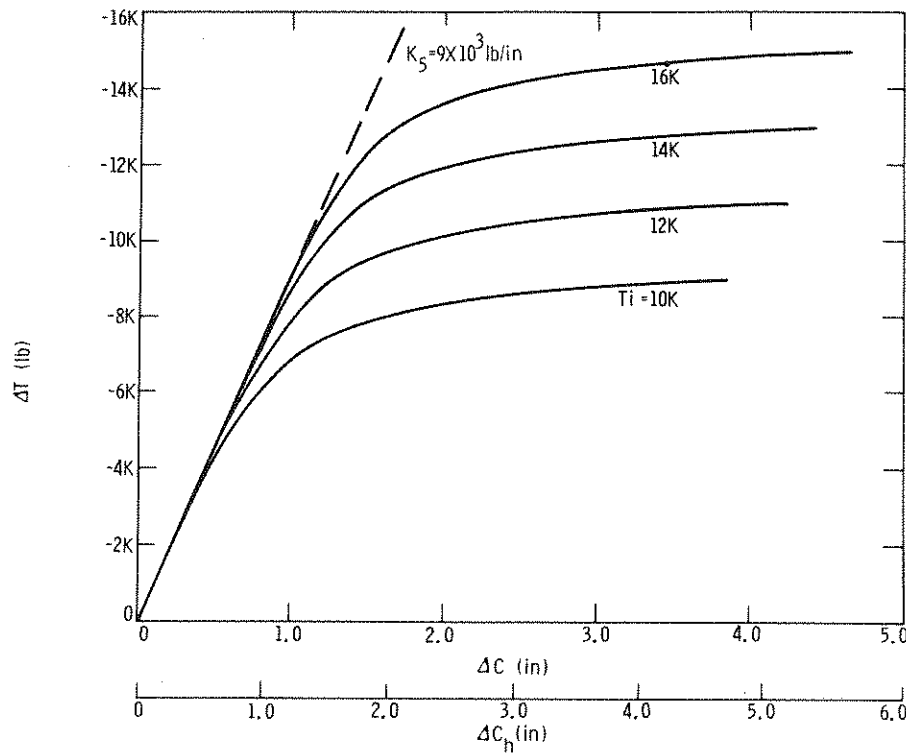


Figure 41. Tension Change vs Deflection

Two additional figures are useful. Figure 42 shows the dependence of final cable tension,  $T_f$ , on  $\Delta c$  and  $\Delta c_h$  and Figure 43 shows the dependence of the cable sag at the strike point,  $\delta_p$ , on the deflections. Results in both figures are presented for various values of initial cable tension. Note, in Figure 43, that for a given initial tension,  $T_i$ , the final sag,  $\delta_p$ , increases rapidly with displacement. This suggests that selection of initial cable tension be based on a minimum acceptable clearance between the sagging cable and a passing blade. For example, if this minimum clearance is selected as 3 feet of separation in the vertical direction, approximately 1 foot may be due to cable sag after tower deflection (the rest would be an allowance for blade deflection and rigid body separation). From Figure 43, if a horizontal tower deflection,  $\Delta c_h$ , of 2.5 inches is allowed (conservatively) then for a strike point sag to be 1 foot or less, the initial cable tension should be 12,000 lb or more. If a deflection,  $\Delta c_h$ , of 3 inches is allowed, then 16,000 lb or more of initial cable tension is required to keep the strike point sag 1 foot or less. For the 17 meter turbine, a 12,000 lb initial cable tension is selected.

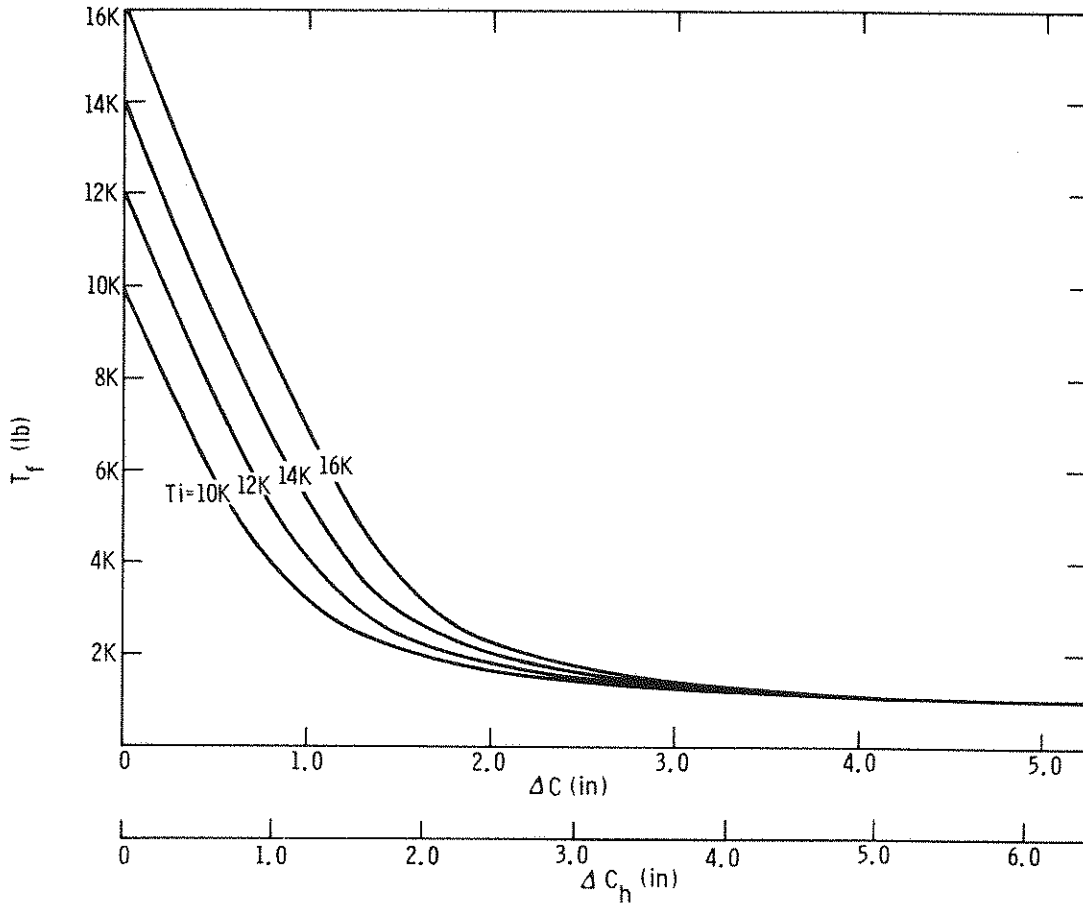


Figure 42. Final Cable Tension vs Horizontal Tower Deflection and Cable Chord Length Change

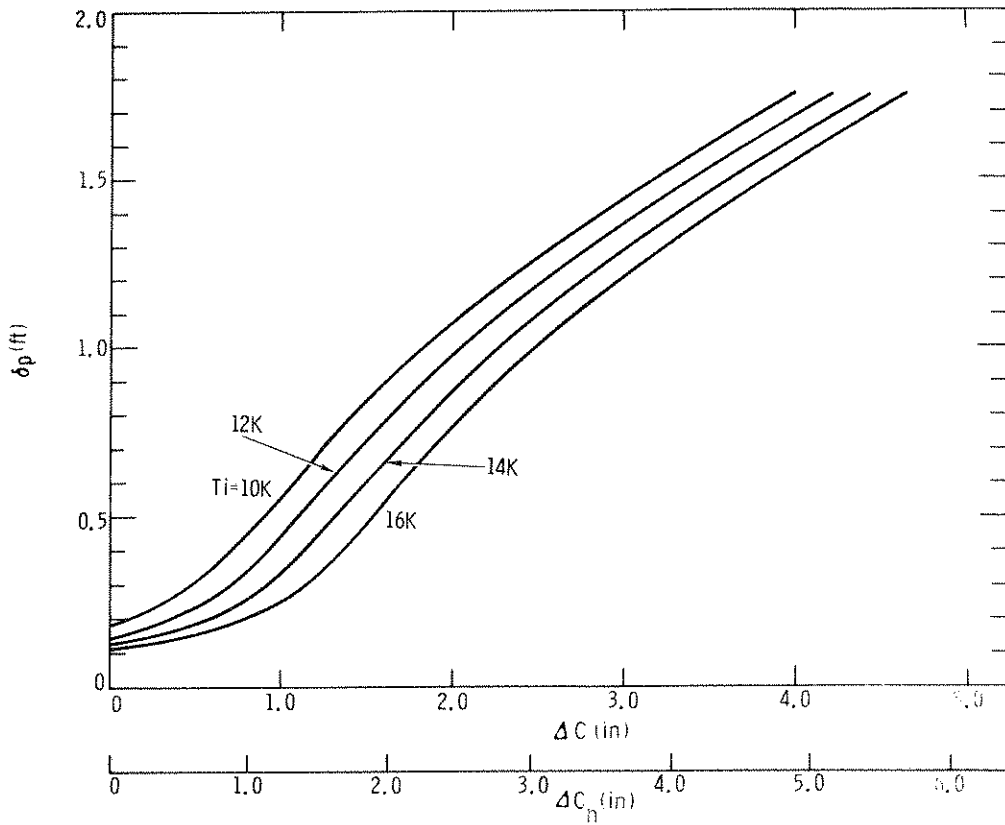


Figure 43. Strike Point Sag vs Horizontal Tower Deflection and Cable Chord Length Change

While the initial cable tension-cable sag-tower deflection interaction can be highly non-linear, proper selection of cable properties and initial tension for a specified performance can practically eliminate the nonlinearities. Since tower deflection, under steady state conditions, is a function of wind speed, it is possible to ease cable tension under lightwind conditions (from a tension value selected to cover all wind possibilities) thereby reducing bearing loads and life. It may also happen that undesirable dynamic effects in the cables may arise under certain operating conditions. In this case, cable tension may have to be adjusted to "detune" the cables.

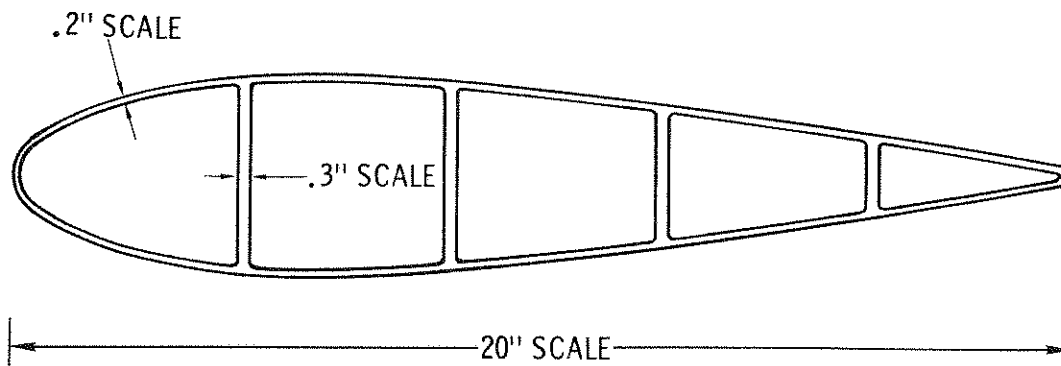
## V. MECHANICAL DESIGN

### Low Cost Blade Fabrication Studies

The low cost blade design effort has been confined to the identification of design approaches which are consistent with the long term goals of low cost at high volume production. Several manufacturers in the metals forming areas show continuing interest although it is apparently time that we give industry some positive signal that we seriously intend to fund such activities.

The applicability of several candidate blade designs was enhanced by the revelation at the VAWT Technology Workshop (May 1976) that a quarter-chord center of gravity was not to be a strict design requirement for the blades. This allows for heavier (and consequently stronger and stiffer) aft blade structure. This, in turn, promotes a manufacturing method which had been thought earlier to be impractical, i. e., extruding a one piece blade from aluminum alloy.

It is feasible to extrude a one-piece blade with an upper state-of-the-art limit of chord length of about 30 inches and with a possible extended limit of 36 inches. The cross section of such a blade would be similar to that shown in Figure 44. After being extruded, the blade would be bent to the desired curve by incremental cold forming techniques or by the stretch-forming process. Structural reinforcements could be provided at the blade ends by adhesive bonding, but this and other end attachment schemes require further analyses.

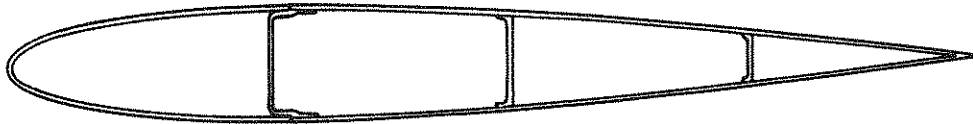


#### FEATURES:

- ONE PIECE ALUMINUM EXTRUSION
- BONDED END REINFORCEMENTS
- COLD BENT TO SHAPE AT SITE
- HIGH TECHNOLOGY - HIGH VOLUME

Figure 44. Extruded Aluminum Blade

A second low-cost blade design incorporating roll-formed components is presented in Figure 45. This design was presented in the May VAWT meeting and met with acceptance by representatives of the roll-forming industry. This design has been little changed except that for structural loading and ease of fabrication considerations, it is probably advisable to increase the thicknesses of the aft structure components. The roll-forming specialists proposed a simplified manufacturing technique which eliminates the stretch-forming sequence to produce the curved portion of the blade.



#### FEATURES:

- ROLL FORMED COMPONENTS
- AUTOMATIC SEAM WELDS
- LOW ALLOY STEEL
- STRETCH-FORMED TO CURVE
- INVESTMENT CAST END FIXTURES
- HIGH TECHNOLOGY-HIGH VOLUME

Figure 45. Blade With Roll-Formed Components

It may be practical to produce the blade component forms desired (already in the curved shape) directly from the roll-forming machines. A present approach for items with small bending radii is to produce continuous close-pitch spiral forms which are then segmented to make items such as bicycle wheel rims. The use of this technique for producing large curved wind turbine blades is an extension of the present state-of-the-art and the industry representatives indicate optimism concerning both the technical feasibility and the economic considerations of such an approach.

A detailed comparison of the two candidate designs included is premature but a few constraints can be noted. The size limit for the extrusion process (chord of 3 feet) is offset by a similar restriction in the roll-forming industry of a raw material width (roll stock) of about 3 feet. This would permit a blade similar to that shown in Figure 45 with a chord of about 4.5 feet. From a manufacturing viewpoint, the roll-formed design is not as restricted as the extrusion design in the choice of materials. The extrusion design will be restricted to several aluminum alloys with good extrusion properties. It is anticipated that each of these designs will be acceptable from a performance standpoint, and that the economics of selection will be based on both the sizes required and the number of blades to be produced.

Both of these metal monocoque designs can be manufactured with techniques that either exist or are very near the present state-of-the-art. Both take advantage of the VAWT allowing a constant airfoil cross-section. Input from the appropriate industries has been considered for these preliminary selections, and each is a good candidate for the task at hand. While the initial cost expectations are encouraging, it remains for industry to undertake a detailed study and development program which will yield reliable cost projections. It is recommended that we fund manufacturability studies for those manufacturing specialties that are either expanding the present state-of-the-art or are unique to our requirements. These studies would be primarily concerned with the difficulties encountered in producing the curved airfoil shape.

Finally, it must be reiterated that the proposed designs are considered target designs only. Follow-on designs which meet operational requirements with lower cost are desirable. We encourage proposals from those industries involved with other manufacturing methods, especially those which incorporate nonmetal materials such as plastics, fiberglass and filament winding.

#### Kaman 17 Meter Blade Contract

Blades for the 17 meter turbine are being designed and fabricated by Kaman Aerospace, Bloomfield, Connecticut. During the period from April to June, 1976, several milestones were reached. Profile geometry of the blades (the blade shape when viewed in the chordwise direction) was finalized. This included placing centerlines of the blade attachment to the tower pins at a radius of 14 inches from the turbine axis for both the straight sections and the struts. Kaman changed the original profile geometry somewhat to permit approximately 13 inches of straight blade to be fabricated at each spanwise end of the circular arc section. They felt it would be easier to bond blade attachment fittings to a straight section than a curved one, thus producing a stronger joint.

Airload predictions and stress calculations were essentially completed during this period. While no serious design problems resulted from the numerical evaluation of the blade stresses for the design conditions, one design change was made to more closely satisfy one of the performance specifications. The specification of interest was a requirement that all blade natural frequencies be above  $3/\text{rev}$  at  $75 \text{ rpm} + 20\%$ ; that is, above 4.5 hz. The Kaman design as originally proposed placed the lowest natural frequency (that corresponding to the first lead-lag mode) at approximately 2.5 hz. The design change made by Kaman was to replace the original 1.5" wide (chordwise direction) trailing edge spline with one 2.8" wide. This was done to add chordwise bending stiffness to the blade section and thus raise the lowest natural frequency from 2.5 hz to about 3.2 hz. While this value does not satisfy the original  $3/\text{rev}$  at  $75 \text{ rpm} + 20\%$ , it is above  $3/\text{rev}$  at  $52 \text{ rpm} + 20\%$ , where 52 rpm is the maximum synchronous operating speed to be used.

During this period the Kaman and Sandia predictions of airloads (therefore stresses) did not agree closely, especially at large values of turbine radius. Sandia's lead-lag loads are approximately twice as large as Kaman's predictions and our flatwise loads are about 50% higher than

Kaman's. After both Sandia and Kaman spent some time trying to resolve the disagreement, it was decided that due to the state-of-the-art of VAWT airload predictions, it would be unproductive to spend more time trying to resolve the disagreement without more field experience, and that Kaman, who has design responsibility for this set of blades, should decide which airloads to use.

Other items accomplished include initiation of ingot procurement for extrusion components, resolution of design details related to end fittings, determination of modal bending moments and establishment of tower-blade interface requirements. A new delivery schedule was given to Sandia.

Nonrecurring engineering	16 July 1976
Tooling	7 September 1976
One set VAWT blades	15 December 1976

Design technical difficulties and Alcoa's extrusion delivery schedule are quoted as being responsible for the delay from the original delivery date of 15 October 1976.

#### Mechanical Design, 17 Meter

The base tower of the VAWT supports the VAWT weight, guy cable loads, and operating loads. The base tower is constructed of welded structural steel angle with legs of 6 x 6 x 0.5 inch angle and side braces of 4 x 4 x 0.375 inch angle. The base tower is eight feet square at the base, tapers to three feet square at the top, and is eleven feet high.

The base tower is bolted to a steel reinforced concrete base that is eleven feet square, four and one-half feet thick, and weights 80,000 pounds. The top of the base tower contains a Timken roller bearing with a 500 rpm rating of 89,500 pounds of vertical thrust and 53,000 pounds of radial loading. This bearing supports the VAWT vertical loads. Three feet below this bearing is another Timken roller bearing with a 500 rpm rating of 33,400 pounds vertical thrust and 48,500 pounds of radial loading. These bearings mount the bottom shaft of the VAWT to the base tower to form the foundation for the rest of the VAWT.

The bottom shaft is an eight foot long steel shaft with a 30.5 inch diameter flange on the top end for mounting the blade shaft, and diameters from eleven to six inches along the rest of the shaft. The shaft has an inside diameter of 2.25 inches for instrumentation cables.

The moving discs of the braking system are attached to the upper part of the bottom shaft and the stationary brake calipers are attached to the top of the base tower.

The blade shaft is bolted to the top flange of the bottom shaft at a height of fifteen feet above the concrete base, and extends beyond this point for another 53 feet to a height of 68 feet. The blade shaft is a steel tube with a twenty-inch outside diameter and one inch wall thickness. A 30.5 inch diameter flange is welded to each end of the blade shaft. The blade struts are attached

to the center of the blade shaft and the blades are attached to the top and bottom shafts. The blade struts are attached to the shaft in an absolute location while the blade attachments are provided with shims to permit vertical adjustment.

The top shaft is a seven foot long steel shaft with a 30.5 inch diameter flange on the bottom end and outside diameters which vary incrementally from eleven to eight inches along the rest of the shaft. A set of Timken roller bearings, identical to the set on the bottom shaft, supports the top shaft and the stationary bearing holder that provides an attachment for the guy cables. The top of the VAWT is 75 feet from the concrete base.

The four guy cables are attached to the top of the VAWT and to four anchors of steel reinforced concrete, which cause the cables to make an angle of 35 degrees with the horizontal. The cable tension will be established at 6,000 pounds by the use of a load cell in each cable. The cables are 129 feet long and are attached to anchors 107 feet from the VAWT vertical centerline. The vertical load on the VAWT from the 4 guy cable tension loads is 14,000 pounds.

The vertical load on the thrust bearing due to the turnbuckles on the bottom radial bearing is 3,000 pounds.

The weights of the VAWT rotating parts follow

<u>Item</u>	<u>Part</u>	<u>Weight-lbs</u>
1	torque sensor	150
2	flex couplings	700
3	bottom shaft	2500
4	bearings	250
5	brake discs	850
6	blade shaft	11500
7	blades	2550
8	blade mounts	2100
9	top shaft	2500
10	shafts, pulleys, etc.	<u>600</u>
	total	23700

The weights of VAWT components follow:

<u>Item</u>	<u>Component</u>	<u>Weight-lbs</u>
1	speed increaser	670
2	right angle gearbox	150
3	generator	500
4	clutch	80
5	motor	<u>300</u>
	total	1700

The weights of the VAWT stationary parts follow:

<u>Item</u>	<u>Part</u>	<u>Weights-lbs</u>
1	top guy cable and bearing mount	1450
2	guy cables	1100
3	brake calipers and mounts	1100
4	bearings	250
5	bottom bearing mounts	350
6	base tower	4000
7	speed increaser tower	500
8	mounting plates	2300
9	brackets, seals, etc.	<u>550</u>
	total	11600

The total VAWT weight = 37000 lbs.

The bottom thrust bearing load follows:

<u>Item</u>	<u>Part</u>	<u>Load-lbs</u>
1	cable tension-vertical	14000
2	bearing and guy cable mount	1500
3	cables	1100
4	top shaft	2500
5	bearings	500
6	blade shaft	11500
7	blades	2550
8	blade mounts	2100
9	brake discs	850
10	bottom shaft	2500
11	bottom bearing mount	350
12	turnbuckle loads-vertical	3000
13	flex coupling	<u>350</u>
	total	42800

#### Turbine Braking System, 17 Meter

Turbine Response to Braking -- The dynamic response of the system to a braking torque is a function of the braking torque, moment of inertia, and wind induced torque. The moments of inertia of various system components were calculated to be the following:

Blades and Struts - 23360 sl ft<sup>2</sup>

Turbine, shaft, and attachments - 463 sl ft<sup>2</sup> above speed increaser

All high speed rotating equipment - 10 sl ft<sup>2</sup>

At 75 rpm the maximum wind induced torque is 40,000 ft-lb. The emergency and proportional brakes are sized to overcome this torque with each system capable of delivering 50,000 ft-lb of torque. The governing equation for the system response to the brake torque is:

$$I \frac{dw}{dt} = T_{\text{wind}} - T_{\text{brake}}$$

Several solutions to this equation are plotted in Figure 46. The "max wind" curves correspond to the condition where the wind speed is such to maximize the wind torque at the turbine RPM. The low inertia case corresponds to the decoupling of the high speed rotating equipment from the turbine shaft and the high inertia case corresponds to the coupling remaining intact. The max wind high inertia case imposes the greatest energy dissipation load on the braking system. ( $2.26 \times 10^6$  ft lb<sub>f</sub>). The energy dissipating ability of a single rotor has been conservatively estimated at  $4.00 \times 10^6$  ft lb<sub>f</sub>. The maximum turbine deceleration occurs at the end of the brake cycle and is  $dw/dt = 2.1$  rad/sec<sup>2</sup> (20 rpm/sec) in the low inertia case ( $dw/dt = 1.5$  rad/sec<sup>2</sup> in the high inertia case).

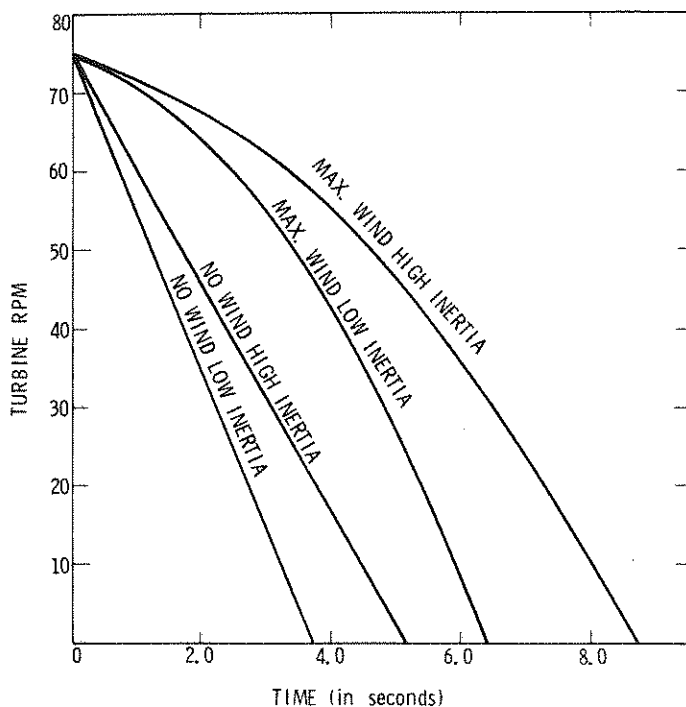


Figure 46. Braking Response Curves

Mechanical Design -- The braking system will use hydraulically-actuated disc brakes placed directly on the output shaft of the turbine above the base unit. Two identical brake rotors will be used: one for the emergency brake, and one for the proportional brake system.

The emergency brake system is designed to supply a constant preselected braking torque to the system. The system can be actuated by a signal from the turbine minicomputer or manually.

by push button contacts located both on the turbine pad and in the control room. In the event of a loss of power the system automatically actuates.

The proportional braking system can be used as an aid in synchronizing the turbine to the electrical network and for routine stopping of the turbine. It also has the capability to serve as the turbine "parking" brake. The system will supply a variable braking torque to the turbine with the torque being controlled through a potentiometer in the control room. A mechanical schematic of the braking system is shown in Figure 47. The upper half of the schematic illustrates the emergency braking system. It is designed to function as follows:

- a. The system is filled with hydraulic fluid through the air fluid reservoir with Valve A in the position shown in the schematic.
- b. The nitrogen bottle is attached and the system pressurized with dry nitrogen. The pressure in the line from the bottle is 200 psi. Valves C are closed and Valve H open. This allows nitrogen to flow through Regulator C establishing a pressure of 20 psi on the nitrogen side of the power booster. Valve D is in the position shown on the schematic and Valve A is in the position opposite that illustrated on the schematic. The hydraulic fluid is thus pressurized to 200 psi in the line from the booster to Valve A and is at atmospheric pressure in the brake lines.
- c. This configuration is the "charged" position of the system and the pressures will remain static for extended periods of time (weeks).
- d. The brakes are applied by de-energizing Valves A and C which places A in the position shown on the schematic and opens Valve C. Nitrogen at 150 psi is thus allowed to flow through Regulators A and B into the power booster. The booster pressurizes the hydraulic fluid to 1500 psi and this pressure is applied to the brakes through Valve A.
- e. The brakes are released by energizing Valve A venting the brake lines to the atmosphere. The pressure in the power booster is reduced by opening Valve B and Closing Valves C and H. Valve D is then energized forcing hydraulic fluid into the system and displacing the booster ram back to its original position.
- f. Valve D is de-energized, Valve B closed, and Valve H opened. This restores the system to the conditions of Step 2.

The proportional and parking brake system is completely independent of the emergency park system and is shown in the lower half of the schematic. When Valve E is in the position shown on the schematic, the system provides a braking torque proportional to the pressure modulated by Value K. In the parking mode of operation the accumulator is first pressurized to 500 psig by controlling Valves I and K. Valve E is then de-energized and shifts into the position opposite that shown in the schematic. In this position, the accumulator supplies pressure to the brake calipers and the parking brake is set.

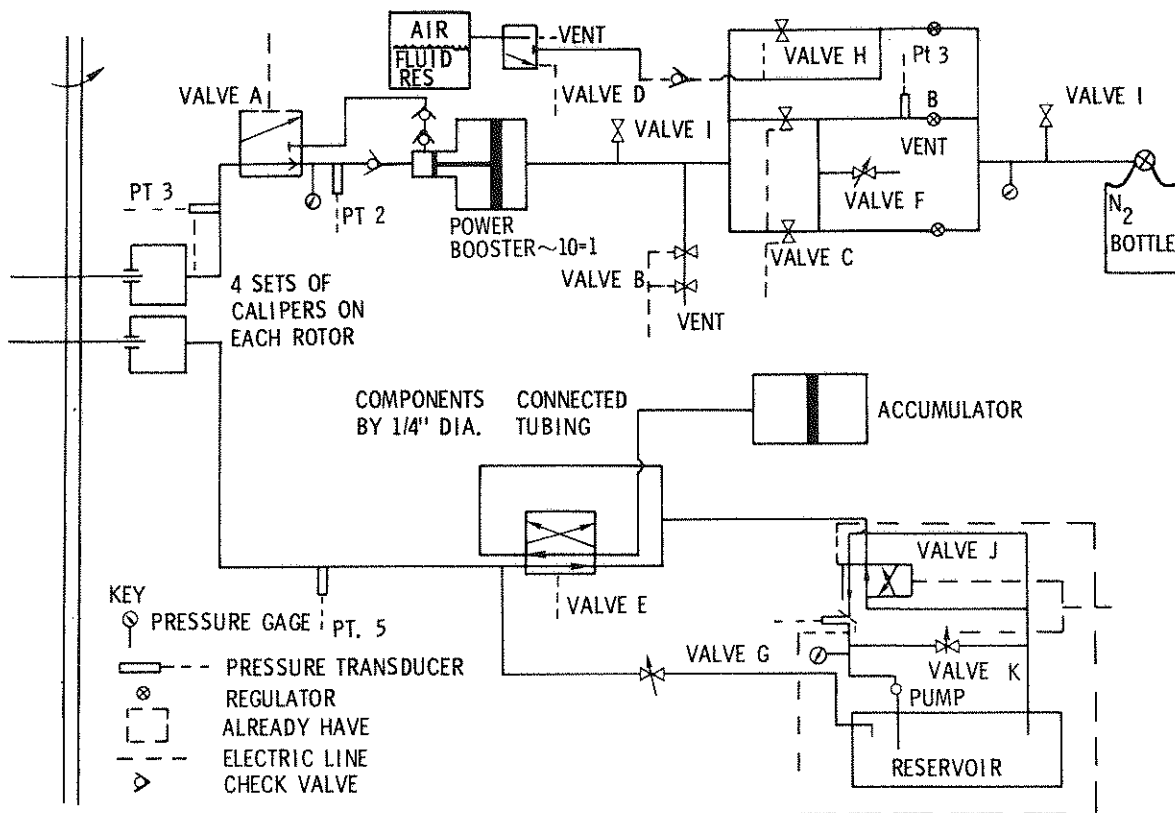


Figure 47. Braking System Schematic

All valves and associated equipment for the emergency brake system will be located in the catwalk area immediately below the brake rotors with the exception of the nitrogen bottle which will be situated adjacent to the hydraulic pump on the pad. The valves, accumulator, and pressure gauges for the proportional brake system will be located adjacent to the pump at the base of the turbine.

### Electrical Design

Figures 48 and 49 are schematics of the brake electrical system, and Figure 50 illustrates the control panel for the system. In the event of a loss of power or malfunction indication from the turbine minicomputer, the emergency brakes will be activated. Manual actuation of the emergency brakes is possible with three emergency push buttons. One of these will be located on the control console, one at the turbine base and one on the turbine catwalk. Relays on the brake circuitry monitor the condition of the brakes. The output from these relays will be used to assure that the turbine is operating in a safe condition. (For example, the turbine cannot be started if the emergency brake system is not charged.)

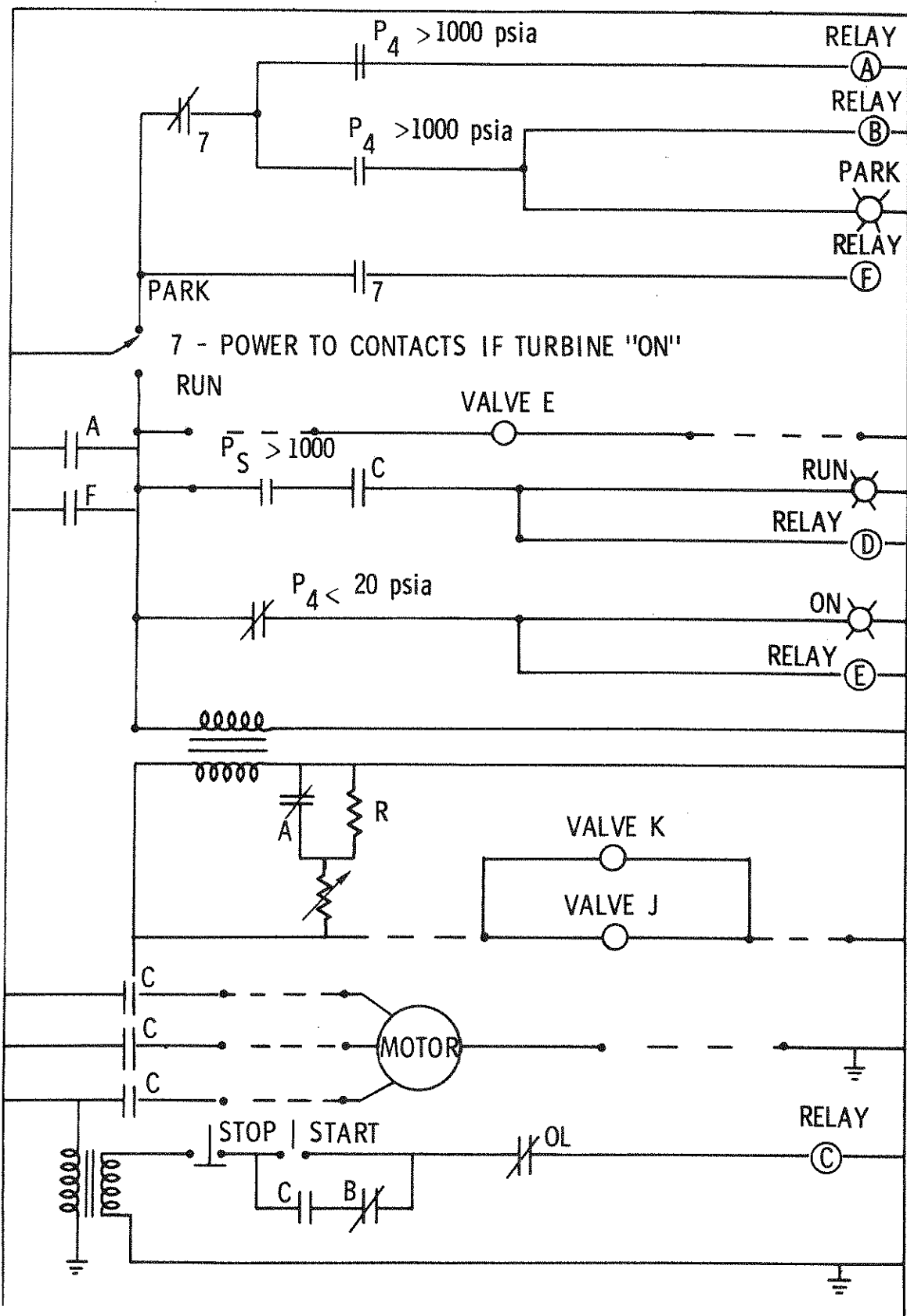


Figure 48. Proportional Brake Electrical System

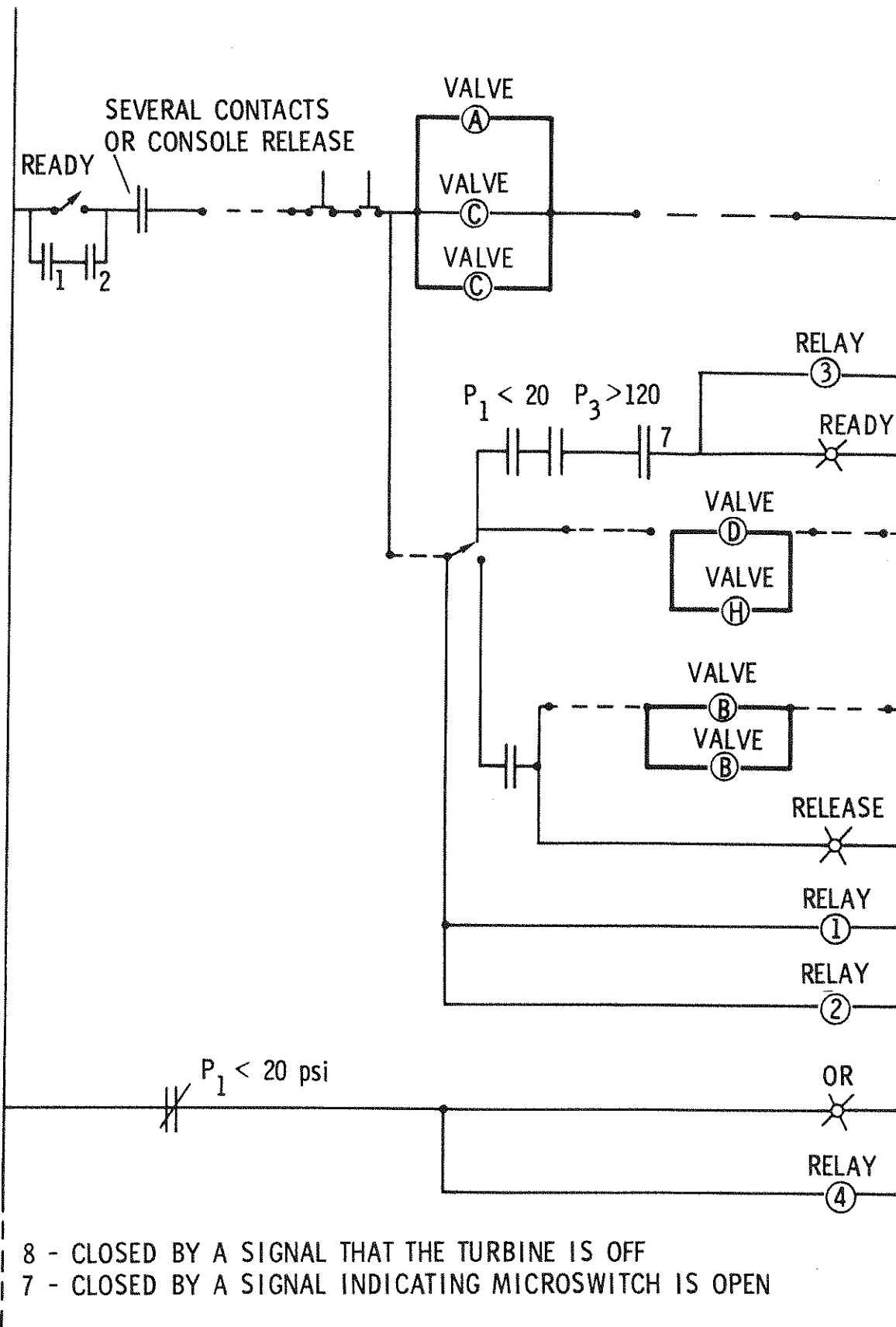
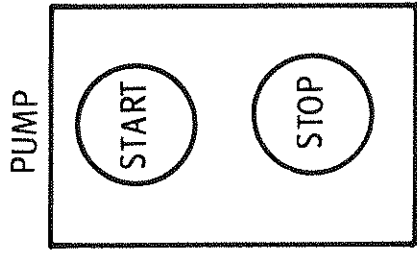
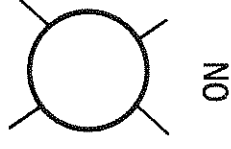
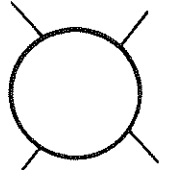
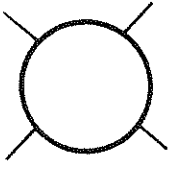
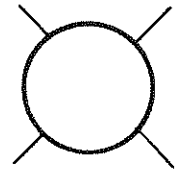
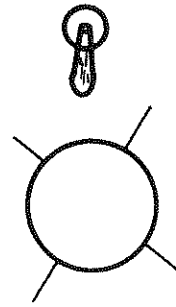
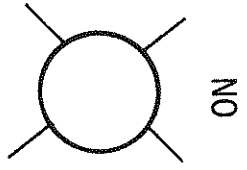
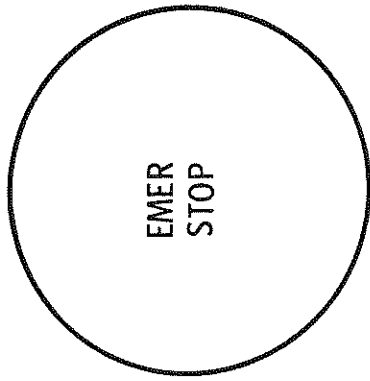
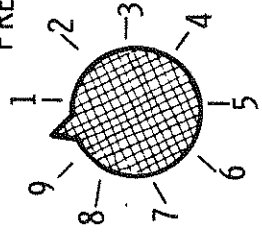


Figure 49. Emergency Brake Electrical System

EMERGENCY BRAKE      PROPORTIONAL



BRAKE PRESSURE



0	5	0
---	---	---

CHARGING PRESSURE

0	1	5	0
---	---	---	---

Figure 50. Brake Control Panel

## VI. VERTICAL-AXIS WIND TURBINE TECHNOLOGY WORKSHOP PROGRAM

### I. PROGRAM OVERVIEWS

Federal Wind Energy Program  
L. V. Divone, ERDA

Large Experimental Wind Turbines - Where We Are Now  
R. L. Thomas, Lewis Research Center

Vertical-Axis Wind Turbine Program  
R. H. Braasch, Sandia Laboratories

Electric Power Research Institute Program  
Piet Bos, EPRI

Canadian Wind Energy Program  
R. J. Templin and P. South, NRC of Canada

### II. ERDA'S DARRIEU VERTICAL-AXIS WIND TURBINE PROGRAM

#### (System Engineering)

System Design - 17-Meter Research Turbine  
E. G. Kadlec, Sandia

System Engineering - Performance Considerations  
W. N. Sullivan, Sandia

Economic Considerations  
J. F. Banas, Sandia

#### (Aerodynamics - Analysis and Testing)

Aerodynamics of the Darrieus Turbine  
J. H. Strickland, Texas Tech University

Selected Wind Turbine Test Results  
B. F. Blackwell, Sandia

Aerodynamics of Four Symmetrical Airfoil Sections  
R. E. Sheldahl, Sandia

5 m Turbine Field Testing  
W. N. Sullivan, Sandia

Performance Prediction for the 17 m Turbine  
J. F. Banas, Sandia

#### (Structural Design)

Structural Overview  
R. C. Reuter, Jr., Sandia

Structural Loads for the 17 m Darrieus Turbine  
W. N. Sullivan, Sandia

Blade Structural Analysis  
L. I. Weingarten and D. W. Lobitz, Sandia

Tower Analysis  
R. C. Reuter, Jr., Sandia

System Structural Response  
J. H. Biffle, Sandia

Effects of System Imbalance  
R. Rodeman, Sandia

Aeroelastic Analysis of the Troposkien-Type Wind Turbine  
N. D. Ham, Massachusetts Institute of Technology

Blade Design and Fabrication of 17 m VAWT  
J. J. Barzda, Kaman Aerospace Corp.

Low-Cost Blade Design Considerations  
L. V. Feltz, Sandia

(Electrical Subsystem, Control and Data Acquisition)

Electrical Power System  
A. F. Veneruso, Sandia

Automatic Control and Data Acquisition  
A. F. Veneruso, Sandia

Anemometry Data and Processing  
J. W. Reed, Sandia

BANQUET ADDRESS--Wind Power, Fact or Fantasy  
W. L. Donaldson, Southwest Research Institute

### III. PROMINENT VERTICAL-AXIS WIND TURBINE PROGRAMS

Aerodynamics of the Darrieus Rotor  
R. E. Wilson, Oregon State University

Darrieus Structural Studies  
R. W. Thresher and E. E. Meyer, Oregon State

Commercial Vertical-Axis Wind Turbines  
L. H. J. Maile, Dominion Aluminum Fabricating, Ltd.

Feasibility Investigation of the Giromill  
R. V. Brulle, McDonnell Aircraft Company

Innovative Wind Machines - Theoretical Performance  
J. B. Fanucci and R. E. Walters, West Virginia University

### IV. REPORTS OF THE WORKING GROUPS

Chairman: R. E. Wilson  
Oregon State University

Chairman's Closing Statement  
L. V. Divone, ERDA

## VII. WORKSHOP ATTENDEES

Ai, Daniel K.  
Senior Scientific Assoc.  
Alcoa Tech. Center  
(Aluminium Composites of America)  
Alcoa Center, PA 15069

Aimone, Anthony F.  
c/o Ceasar Aimone  
200 Fifth Street  
Iron Mountain, MI 49801

Andrews, Carl  
Altruistic Communities  
Project Engineer  
110 E. Anaheim  
Long Beach, CA 90813

Banas, James - 5742  
Sandia Laboratories  
Albuquerque, NM 87115

Barieau, Dr. Robert  
Research Professor  
West Texas State Univ.  
Box 248, W. T. Station  
Canyon, TX 79016

Barzda, Justin  
Chief of Systems Research  
Kaman Aerospace Corporation  
Old Windsor Road  
Bloomfield, CT 06002

Bea, Karl J.  
Enerjair, Ltd.  
(American Ultramar, Ltd.)  
128 Dewitt Street  
Syracuse, NY 13203

Beckman, Ralph  
REDE Research Institute  
P.O. 212  
Providence, RI 02901

Benjamin, John  
Assoc. Director  
Pollution Control Research Institute  
3875 Jackson Station #19  
Riverside, CA 92503

Bergey, Mike  
University of Okalahoma  
Rt #1 Box 151B  
Norman, OK 73069

Biffle, Johnnie - 1281  
Sandia Laboratories  
Albuquerque, NM 87115

Bill, Donald F.  
Org. CDI  
1080 N. River Drive  
Miami, FL 33136

Blackwell, Ben - 1333  
Sandia Laboratories  
Albuquerque, NM 87115

Bolt, Jan B. D. H.  
Fokker-VFW  
P.O. Box 7600  
Schiphol-cost, The Netherlands  
020/731044

Boland, Joseph F.  
Rockwell International  
Rocky Flats Plant  
Box 474  
Golden, CO 80401

Bos, Piet  
Program Manager, Solar Energy  
Electric Power Research Institute  
3412 Hillview Avenue  
Palo Alto, CA 94303

Braasch, R. H. - 5715  
Sandia Laboratories  
Albuquerque, NM 87115

Braz, John  
TCHUBA  
98 Camp Street  
Providence, RI 02906

Breed, Robert A.  
Wood World  
579 Calle Dia  
Carpinteria, CA 93013

Brulle, Robert V.  
Giromill Project Manager  
McDonnell Aircraft Co.  
P.O. Box 516, Dept. 241, Bldg. 32  
St. Louis, MO 63166

Carlin, Palmer  
Colorado University  
Professor Electrical Engineering  
2209-4th Street  
Boulder, CO 80302

Carlis, Bill  
Southwest Energy Options  
109 W. California Street  
Silver City, NM 88061

Ceiderburg, John W.  
Ceiderburg Engineering  
Box 259  
Aptos, CA 95003

Charron, R.  
The American Committee for Cape Verde  
14 Beacon Street  
Boston, MA 02108

Clark, John M.  
Institute of Arctic Apline Research  
University of Colorado  
Boulder, CO 80309

Cole, Alan L.  
Northern Illinois University  
Dept. of Geography  
DeKalb, IL 60115

Craik, Darrel W.  
Teledyne Aero-Cal  
523 E. Mission Road  
San Marcos, CA 92069

Cromack, Duane E.  
Dept. of Mechanical Engineering  
University of Massachusetts  
Amherst, MA 01002

Davenport, Steven R.  
Oklahoma State University  
900 N. Portland  
Oklahoma City, OK 73107

Davitian, Harry  
Brookhaven National Laboratory  
Bldg. 475  
Upton, NY 11973

Dennis, Tom L.  
Brunswick Corporation  
504 Sweetwater Blvd.  
Longwood, FL 32750

Dhande, Sanjay G.  
Mechanical Engineering Dept.  
University of Florida  
Gainesville, FL 32677

Divone, Louis V.  
Chief, Wind Energy Conversion Branch  
Division of Solar Energy  
Energy Research and Development Admin.  
Washington, DC 20545

Dodge, Robert J.  
Automatic Power, Inc.  
213 Hutcheson Street  
Houston, TX 77003

Donaldson, W. Lyle  
Senior Vice President  
Southwest Research Institute  
P.O. Drawer 28510  
San Antonio, TX 78284

Dorn, Dave W.  
Lawrence Livermore Laboratory  
P.O. Box 808  
Livermore, CA 94550

Dougan, David  
Hamilton Standard  
Area Representative  
Box 58096  
Houston, TX 77058

Drake, William E.  
Enertech Corporation  
P.O. Box 420  
Norwich, VT 05055

Drees, Herman M.  
Pinson Energy Corporation  
76 Ashford Street  
Allston, MA 02134

Dunitz, Margie  
University of Michigan  
1620 Cambridge Rd.  
Ann Arbor, MI 48104

Espeset, Nick  
Foundation for Rural Technology  
903 Pine Street  
Boulder, CO 80302

Fanucci, Jerome B.  
Professor and Chairman  
Dept. of Aerospace  
West Virginia University  
Morgantown, WV 26506

Fekete, G. I.  
Asst. Assoc. Professor  
McGill Univ.  
Montreal, Canada

Feltz, Louis - 1324  
Sandia Laboratories  
Albuquerque, NM 87115

Francis, Serre  
Rohn Manufacturing Co.  
P.O. 23428  
San Jose, CA 95153

Frenchman, R. M.  
The American Committee for Cape Verde  
14 Beacon Street  
Boston, MA 02108

Fuller, Gerald  
University of Regina  
Faculty of Engineering  
Regina, Canada

Gillies, Alan  
University of Oklahoma  
209 Cedar Lane  
Moore, OK

Gilmore, Earl H.  
WTSU-AC-SIGMA  
Rt 1 Box 430  
Amarillo, TX 79106

Gordon, Robert  
Structural Composites Industries, Inc.  
6344 North Irwindale Ave.  
Azusa, CA 91702

Gross, William A.  
Dean, College of Engineering  
University of New Mexico  
107 Farris Engr. Center  
Albuquerque, NM 87131

Grover, Robert D.  
10213 Norman Avenue, NE  
Albuquerque, NM 87112

Groves, Donald J., Jr.  
Public Service Co.  
P.O. Box 2267  
Albuquerque, NM 87103

Hadlock, R. K.  
Battelle Pacific Northwest Laboratory  
P.O. Box 999  
Richland, WA 99352

Ham, Norman D.  
Massachusetts Institute of Technology  
77 Massachusetts Avenue  
Cambridge, MA 02139

Heckman, Ken  
Teledyne Aero-Cal  
528 E. Mission Rd.  
San Marcos, CA 92069

Hill, John M.  
Assoc. Prof. of Civil Engineering  
University of Wyoming  
Laramie, WY 82071

Hill, P. Ward  
Hercules, Inc.  
P.O. Box 210  
Cumberland, MD 21502

Holme, Olof A. M.  
SAAB-SCANIA AB Aerospace Div.  
Linkoping, Sweden S-58188

Hughes, W. L.  
Oklahoma State University  
202 Engineering South  
Stillwater, OK 74074

Johnson, Steven A.  
Wind Energy Association  
4594 Creek View Drive  
Salt Lake City, UT 84107

Jones, Brian H.  
Compositer Engineering Corp.  
6960-5 Aragon Circle  
Buena Park, CA 90620

Jones, Robert  
R&M Ranch, Inc.  
570 N. Lillian Way  
Los Angeles, CA 90004

Jayadev, T. S.  
College of Applied Science  
University of Wisconsin  
Milwaukee, WI 53201

Kadlec, Emil - 5715  
Sandia Laboratories  
Albuquerque, NM 87115

Krug, Edwin H.  
Director, Military Planning  
Lear Siegler, Inc.  
4141 Eastern Avenue SE  
Grand Rapids, MI 49508

Langerman, Lowell  
Rt 2  
Fayette, IA 52142

Larsen, Harold C.  
Air Force Institute of Technology  
AFIT/END, WPAFB  
Dayton, OH 45433

Lechner, T. Michael  
Bovay Engineers, Inc.  
P.O. Box 30068  
Albuquerque, NM 87110

Lefever, Dan  
Sonnwald Service  
Rt #1, Box 457  
Spring Grove, PA 17362

Lefever, Evan  
Route 2, Box 203  
Berkeley Springs, WV 25411

Lefever, Tim  
Sonnewald Service  
Route #1, Box 457  
Spring Grove, PA 17362

Lissaman, Peter  
Aerovironment  
Las Vista  
Pasadena, CA 91107

Ljungstroem, Olle  
N. E. National Swedish Board for Energy  
Source Development  
STU, FACK S-(0072)  
Stockholm 43, Sweden

Lopez, Gilbert  
Bureau of Indian Affairs  
P. O. Box 1248  
Albuquerque, NM 87103

Maile, L. H. J.  
Engineering Manager  
Dominion Aluminum Fabricating, Ltd.  
3570 Hawkestone Road  
Mississauga, Ontario, Canada  
L5C 2V8

Malver, Fred  
Honeywell, Inc.  
2600 Ridgeway Pkwy  
Minneapolis, MN 55413

Matakovich, George J.  
Store, Matakovich & Wolfberg  
715 E. Mission Drive  
San Gabriel, CA 91776

McCarthy, John S.  
McDonnell Douglas Corp.  
345 Gray Avenue  
St. Louis, MO 63119

McClure, Paul  
Asst. Professor of Aerospace Engr.  
University of Texas  
Taylor Hall 227  
Austin, TX 78712

Merriam, Marshal  
Lawrence Berkeley Laboratory  
University of California  
Dept. of Materials Science  
Hearst Mining  
Berkeley, CA 94720

Metcalf, Philip  
Unarco-Rohn  
P. O. Box 2000  
Peoria, IL 61601

Meyer, Hans  
Windworks  
Box 329, Route 3  
Mukwonago, WI 53149

McConnell, Robert  
Institute of Research of Hydro-Quebec  
1800 Montec Ste Julie  
Varrenes, Quebec, Canada JOL 2 PO

Michlin, Steven B.  
University of Michigan  
1620 Cambridge Rd.  
Ann Arbor, MI 48104

Miller, Larry  
Oklahoma State University Technical  
Institute  
900 N. Portland  
Oklahoma City, OK 73107

Mims, Forrest M., Jr.  
UTSA  
234 Five Oaks Drive  
San Antonio, TX 78209

Mitcham, Tina  
Pollution Control Research Institute  
3875 Jackson Station #19  
Riverside, CA 92503

Mortimer, A. J.  
Box 72  
Oldwick, NJ 08858

Nassar, Esam  
Illinois Institute of Technology  
3110 S. State Street  
Chicago, IL 60616

Nelson, Vaughn  
West Texas State University  
Dept. of Physics  
Box 248, W. T. Station  
Canyon, TX 79016

Packard, Lyle E.  
Packard Marine  
505 N. Lake Shore Drive  
Chicago, IL 60611

Palmer, Darwin G.  
701 Wagon Trail, SE  
Albuquerque, NM 87123

Park, Jack  
Helion  
Box 4301  
Sylmar, CA 91342

Pedersen, Bjarne Maribo  
Technical University Denmark  
Danish Academy of Technical Sciences  
Dept. of Fluid Mech.  
Bygn 404 DTH, 2800 Lyngby  
Denmark

Penrod, Robert  
P.O. Box 1047  
Cape Girardeau, MO 63701

Piepers, G. G.  
Reactor Centrum Nederland  
Westerduinweg 3 Petten  
(N. H.) The Netherlands

Ramakumar, Dr. R.  
Assoc. Prof., Electric Engineering  
Oklahoma State University  
202 Engineering South  
Stillwater, OK 74074

Ramos, A. D.  
The American Committee for Cape Verde  
14 Beacon Street  
Boston, MA 02108

Ramsdell, J. V.  
Bettelle Pacific Northwest Laboratory  
Research Scientist  
P.O. Box 999  
Richland, WA 99352

Reed, Jack - 5443  
Sandia Laboratories  
Albuquerque, NM 87115

Reuter, Robert - 5715  
Sandia Laboratories  
Albuquerque, NM 87115

Rodeman, Ronald - 1281  
Sandia Laboratories  
Albuquerque, NM 87115

Rollins, Charles  
Box 737  
El Cerrito, CA

Root, David H.  
U. S. Geological Survey  
Mail Stop 922  
Reston, VA 22092

Sandor, G. N.  
M. E. Dept.  
University of Florida  
Gainesville, FL 32677

Sayler, John P.  
American Energy Alternatives, Inc.  
P.O. Box 905  
Boulder, CO 80302

Scully, Dan  
Total Environment Action  
Box 47  
Harrisville, NH 03450

Seath, Donald D.  
University of Texas at Arlington  
Aerospace Engr. Dept.  
UTA Box 19428  
Arlington, TX 76019

Seaverson, Louis A.  
Rockwell International  
P.O. Box 464  
Golden, CO 80401

Sheehan, John L.  
Chief Engineer  
Sheehan Consultants  
5320 Ken Caryl Rd.  
Littleton, CO 80123

Shepardson, William P.  
Pinson Energy Corp.  
76 Ashford Street  
Allston, MA 02134

Sholes, John E.  
NASA-Lewis Research Center  
21000 Brook Park Rd.  
Cleveland, OH 44135

Skoglund, Victor J.  
University of New Mexico  
ME 101  
Albuquerque, NM 87131

Smith, Brent  
ISTARA Research  
P.O. Box 735  
Boulder, CO 80302

Snyder, Melvin H.  
Wichita State University  
Wichita, KS 67208

Soderholm, L. H.  
USDA-ARS  
Room 213 Ag. Engr.  
Iowa State University  
Ames, IO 50011

South, Peter  
National Research Council of Canada  
Research Office  
Bldg. M-2, Montreal Rd.  
Ottawa, Ontario (Canada) KLA OR6

Stein, Bill  
Natural Power  
Francestown Turnpike  
New Boston, NH 03070

Takanashi, Akihiro  
University of Florida  
Dept. of Mechanical Engineering  
Gainesville, FL 32611

Teague, Don  
Energy Research and Development Admin.  
Washington, DC 20545

Thomann, Gary C.  
Wichita State University  
Wichita, KS 67208

Thomas, Robert  
Wind Harvest Co.  
750 Mission  
Camarillo, CA 93010

Todd, Clement  
U. S. Bureau of Reclamation  
Denver FC Bldg. 67 Room 620  
Denver, CO 80225

Sheldahl, Robert - 1333  
Sandia Laboratories  
Albuquerque, NM 87115

Strickland, James H.  
Mechanical Engineering Department  
Texas Tech University  
Lubbock, TX 79409

Sullivan, William N. - 1284  
Sandia Laboratories  
Albuquerque, NM 87115

Templin, R. J.  
Head, Low Speed Aerodynamics Lab  
National Research Council (Canada)  
Montreal Road  
Ottawa, Canada K1H 6R6

Thomas, Ronald L.  
Head, Windpower Office  
NASA-Lewis Research Center  
21000 Brookpark Road  
Cleveland, OH 44135

Thresher, Robert W.  
Associate Professor  
Mechanical Engineering Department  
Oregon State University  
Corvallis, OR 97331

Veneruso, Anthony - 5715  
Sandia Laboratories  
Albuquerque, NM 87115

Walters, Richard E.  
Associate Professor of Aerospace Engineering  
West Virginia University  
Morgantown, WV 26506

Weingarten, Larry - 1284  
Sandia Laboratories  
Albuquerque, NM 87115

Wilson, Robert E.  
Professor, Mechanical Engineering Dept.  
Oregon State University  
Corvallis, OR 97331

Tsao, Peter  
Northern Illinois University  
Physics Dept.  
DeKalb, IL 60115

Turnquist, Ralph O.  
Kansas State University  
1100 Pioneer Lane  
Manhattan, KS 66502

Van Dalen, Gerritt  
FDO-Engineering Consultants  
P.O. Box 194  
Hengelo, Netherlands

Warchol, Edward J.  
Bonneville Power Administration  
P.O. Box 3621  
Portland, OR 97208

Weeks, Stanley A.  
Agricultural Engineering Department  
Cornell University  
312 Agr. Engr. Dept.  
Ithaca, NY 14853

Werner, Charles  
Unarco-Rohn  
Sales and Engr. Department  
P. O. Box 2000  
Peoria, IL 61601

Wood, Rhonde Paul  
1180 Alvarado, SE #208  
Albuquerque, NM 87108

Worstell, Mark  
University of Oklahoma  
1319 S. Jenkins - Apt. B  
Norman, OK 83069

Zweig, Pete R.  
Associate Director  
Pollution Control Research Institute  
3875 Jackson Station #19  
Riverside, CA 92503

VIII. SANDIA PUBLICATIONS AND PRESENTATIONS  
(April-June 1976)

SAND76-5536 Proceedings of the Vertical-Axis Wind Turbine Technology  
Workshop, Albuquerque, NM, May 17-20, 1976.

Presentations

R. H. Braasch, "Wind Power," New Initiatives Colloquium, Sandia Laboratories, Albuquerque, NM, January 7, 1976.

R. C. Reuter, "Sandia Wind Energy Program," American Institute of Architects, Albuquerque, NM, February 19, 1976.

J. F. Banas, W. N. Sullivan, "Application of Wind Turbines for the Generation of Electrical Power," ASME Symposium on Energy Alternatives, Albuquerque, NM, February 26, 1976.

A. F. Veneruso, "Wind Power - The VAWT and Plant Engineering Needs," American Institute of Plant Engineers, Albuquerque, NM, March 5, 1976.

R. H. Braasch, "VAWT Program," Central New Mexico Section of the American Institute of Mining and Metallurgical Engineers, Albuquerque, NM, March 20, 1976.

R. H. Braasch, et al., Vertical-Axis Wind Turbine Technology Workshop, May 17-20, 1976.

## IX. PREVIOUS SANDIA PUBLICATIONS AND PRESENTATIONS

- SAND74-0071 Wind Energy Potential in New Mexico, J. W. Reed, R. C. Maydew, B. F. Blackwell, July 1974.
- SAND74-0100 Practical Approximations to a Troposkien by Straight-Line and Circular-Arc Segments, G. E. Reis, B. F. Blackwell, March 1975.
- SAND74-0105 An Electrical System for Extracting Maximum Power from the Wind, A. F. Veneruso, December 1974.
- SLA-74-0154 Blade Shape for a Troposkien Type of Vertical-Axis Wind Turbine, B. F. Blackwell, G. E. Reis, April 1974.
- SLA-74-0160 The Vertical-Axis Wind Turbine - How it Works, B. F. Blackwell, April 1974.
- SAND74-0177 Some Geometrical Aspects of Troposkiens as Applied to Vertical-Axis Wind Turbines, B. F. Blackwell, G. E. Reis, March 1975.
- SLA-74-0298 A Wind-Powered Fresh Water Condensation Air Conditioning, Mariculture, and Aquiculture Integrated System for Pacific Atolls, D. B. Shuster, V. L. Dugan, R. H. Richards, June 1974.
- SAND74-0348 Wind Power Climatology of the United States, J. W. Reed, May 1975.
- SAND74-0378 Nonlinear Stress Analysis of Vertical-Axis Wind Turbine Blades, L. I. Weingarten, R. E. Nickell, April 1975.
- SAND74-0379 An Investigation of Rotation-Induced Stresses of Straight and of Curved Vertical-Axis Wind Turbine Blades, L. V. Feltz, B. F. Blackwell, March 1975.
- SAND74-0435 Wind Power Climatology, J. W. Reed, December 1974.
- SAND75-0165 Application of the Darrieus Vertical-Axis Wind Turbine to Synchronous Electrical Power Generation, J. F. Banas, E. G. Kadlec, W. N. Sullivan, March 1975.
- SAND75-0166 Wind Energy - A Revitalized Pursuit, B. F. Blackwell, L. V. Feltz, March 1975.
- SAND75-0204 Methods for Performance Evaluation of Synchronous Power Systems Utilizing the Darrieus Vertical-Axis Wind Turbine, J. F. Banas, E. G. Kadlec, W. N. Sullivan, April 1975.
- SAND75-0431 The Darrieus Turbine: A Performance Prediction Model Using Multiple Stream-tubes, J. H. Strickland, October 1975.
- SAND75-0530 Engineering of Wind Energy Systems, J. F. Banas, W. N. Sullivan, January 1976.
- SAND76-0131 Wind Tunnel Performance Data for Two- and Three-Cup Savonius Rotors, B. F. Blackwell, L. V. Feltz, R. E. Sheldahl, to be published.
- SAND76-0036 Sandia Vertical-Axis Wind Turbine Program Technical Quarterly Report: October-December 1975, J. F. Banas, W. N. Sullivan (editors), April 1976.
- SAND76-0130 Blackwell, B. F., Sheldahl, R. E., and Feltz, L. V., Wind Tunnel Performance Data for the Darrieus Wind Turbine with NACA 0012 Blades (U), Sandia Laboratories, Albuquerque, New Mexico, May 1976.

## External Publications

U.S. Patent Number 3,918,839, "Wind Turbine," 16 Claims, B. F. Blackwell, L. V. Feltz, R. C. Maydew, November 11, 1975.

J. W. Reed, "Wind Power Climatology," Weatherwise, 27, 6, December 1974, and SAND74-0435, Sandia Laboratories, December 1974.

J. W. Reed, R. C. Maydew, and B. F. Blackwell, A Report of the Governor's Select Committee on Wind Energy, "Wind Energy Potential in New Mexico," Santa Fe, NM, June 7, 1975.

L. I. Weingarten and R. E. Nickell, "Nonlinear Stress Analysis of Vertical-Axis Wind Turbine Blades," Journal of Engineering for Industry, Transactions ASME, Vol. 97, Series B, No. 4, November 1975, pp. 1234-1237.

## Presentations

J. W. Reed, "Some Notes on Wind Power Climatology," American Meteorological Society Climatology Conference, Asheville, NC, October 8-11, 1974.

L. V. Feltz, "Wind Power - A revitalized Pursuit," Heights Lions Club, Albuquerque, NM February 13, 1975.

B. F. Blackwell, "Wind Energy - A revitalized Pursuit," ASME Resource Recovery Symposium, Albuquerque, NM, March 6-7, 1975.

R. C. Maydew, "Wind Energy," New Mexico State University, Las Cruces, NM, March 14, 1975.

L. V. Feltz, "Wind Power - A Revitalized Pursuit," Sierra Club, University of Colorado, Boulder, CO, March 22, 1975.

J. W. Reed, "Wind Energy Potential in the Southwest," Southwestern Technology Utilization Conference, Albuquerque, NM, April 16-17, 1975.

L. V. Feltz, "Wind Power - A Revitalized Pursuit," New Mexico IEEE Spring Symposium on Energy Research in New Mexico, Albuquerque, NM, April 17-18, 1975.

J. W. Reed, "Wind Power Climatology," New Mexico IEEE Spring Symposium on Energy Research in New Mexico, Albuquerque, NM, April 17-18, 1975.

J. W. Reed, "Wind Power Climatology Research at Sandia Laboratories," 51st Annual American Association for the Advancement of Science Southwestern Division Meeting, Energy Resources Symposium, Los Alamos, NM, April 23-26, 1975.

R. H. Braasch, "Power Generation with a Vertical Axis Wind Turbine," Wind Workshop II, Washington, DC, June 9-11, 1975.

J. W. Reed, "Wind Climatology," ERDA-NSF Wind Energy Conversion Symposium Workshop, Washington, DC, June 9-11, 1975.

J. W. Reed and B. F. Blackwell, "Some Climatological Estimates of Wind Power Availability," 2nd U.S. National Conference on Wind Engineering Research, Ft. Collins, CO, June 23-25, 1975.

B. F. Blackwell and G. E. Reis, "Geometrical Aspects of the Troposkein as Applied to the Darrieus Vertical-Axis Wind Turbine," ASME Paper 75-DET-42, ASME Design Engineering Technical Conference, Washington, DC, September 1975.

A. F. Veneruso, "VAWT Technology," New York Ocean Science Laboratory, Montauk, Long Island, NY, August 20, 1975.

L. V. Feltz, "Wind Energy Potential," Bureau of Indian Affairs, Juneau, Alaska, September 11, 1975.

A. F. Veneruso, "VAWT Technology," United Nations Office of Technical Cooperation, UN Hdqs, NY, September 25, 1975.

L. I. Weingarten, "Nonlinear Stress Analysis of Vertical-Axis Wind Turbine Blades," ASME Paper 75-DET-35, ASME Design Engineering Technical Conference, Washington, DC, September 1975.

R. C. Reuter, "Wind Power," Rio Grande Lions Club, Albuquerque, NM, October 10, 1975.

E. G. Kadlec, "Sandia Wind Power Program," American Wind Energy Association, Santa Rosa, CA, October 11, 1975.

E. G. Kadlec, "Sandia Wind Power Program," Iowa 2000 Conference, Ames, Iowa, October 12, 1975.

A. F. Veneruso, "VAWT Technology and Electrical Considerations for Utilities," Public Service Company of NM, Albuquerque, NM, October 23, 1975.

L. I. Weingarten and L. V. Feltz, "Material and Manufacturing Considerations for the Vertical-Axis Wind Turbine," Seventh National Society for the Advancement of Material and Process Engineering Technical Conference, Albuquerque, NM, October 1975.

E. G. Kadlec, "Sandia Wind Power Program," Industrial College of the Armed Forces, Albuquerque, NM, December 8, 1975.

## X. REFERENCES

1. Banas, J. F., Kadlec, E. G., Sullivan, W. N., "Application of the Darrieus Vertical-Axis Wind Turbine to Synchronous Electrical Power Generation," Sandia Laboratories, SAND75-0165, March, 1975.
2. Sandia Vertical-Axis Wind Turbine Program Technical Quarterly Report, Edited by J. F. Banas and W. N. Sullivan, Sandia Laboratories, SAND76-0036, April 1976.
3. Blackwell, B. F. and Reis, G. E., "Blade Shape for a Troposkien Type of Vertical-Axis Wind Turbine," Sandia Laboratories, SLA74-0154, April, 1974.
4. Blackwell, B. F. and Reis, G. E., "Geometrical Aspects of the Troposkien Shape as Applied to Vertical-Axis Wind Turbines," Sandia Laboratories, SAND75-0177, April, 1975.
5. Strickland, J. H., "The Darrieus Turbine: A Performance Prediction Model Using Multiple Streamtubes," Sandia Laboratories, SAND75-0431, October, 1976.
6. "Design Study of Wind Turbines 50 kW-3000 kW for Electric Utility Applications," Kaman Aerospace Corp., Kaman Report R1382, February, 1976.
7. Ham, N. D., "Aeroelastic Analysis of the Troposkien-Type Wind Turbine, Vertical-Axis Wind Turbine Workshop," Albuquerque, NM, May 17-20, 1976.
8. Sandia Vertical-Axis Wind Turbine Program Technical Quarterly Report, Edited by L. I. Weingarten and B. F. Blackwell, SAND76-0338.
9. Blackwell, B. F., Feltz, L. V., and Sheldahl, R. E., "Wind Tunnel Performance Data for the Darrieus Wind Turbine with NACA-0012 Blades," Sandia Laboratories, SAND76-0130.
10. MIL-HDBK-5B, Metallic Materials and Elements for Aerospace Vehicle Structures, September 1, 1971, Department of Defense.
11. Mechanical Behavior of Engineering Materials, J. Marin, Prentice-Hall, Inc., 1962.
12. "Helicopter Fatigue Load and Life Determination Methods," University of Dayton Research Institute, USAAMRDL-TR-75-27, August, 1975.
13. Miner, M. A., "Cumulative Damage in Fatigue," Trans. A.S.M.E., Vol. 67, 1945.
14. Harris, C. M., and Crede, C. E., Editors, Shock and Vibration Handbook, Vol. 2, p. 24-11.
15. Shears, M., "Static and Dynamic Behavior of Guyed Masts," University of California, Report No. 68-6, Berkeley, California, June, 1968.

DISTRIBUTION:

TID-4500-R65, UC-60 (265)

R. J. Templin  
Low Speed Aerodynamics Section  
NRC-National Aeronautical Establishment  
Ottawa 7, Ontario, Canada K1A0R6

A. Robb  
Memorial Univ. of Newfoundland  
Faculty of Eng. & Applied Sciences  
St. John's Newfoundland  
Canada A1C 5S7

H. Sevier  
Rocket and Space Division  
Bristol Aerospace Ltd.  
P. O. Box 874  
Winnipeg, Manitoba  
R3C 2S4 Canada

V. A. L. Chasteau  
Department of Mech. Engineering  
The University of Auckland  
Private Bag  
Auckland, New Zealand

G. Herrera  
Jet Propulsion Lab  
4800 Oak Grove Drive  
Pasadena, CA 91103

NASA  
Langley Research Center  
Hampton, VA 23665  
Attn: R. Muraca, MS 317

NASA (2)  
Lewis Research Center  
2100 Brookpark Road  
Cleveland, OH 44135  
Attn: J. Savino, MS 509-201  
R. L. Thomas

ERDA Headquarters (20)  
Washington, DC 20545  
Attn: L. Divone, Chief  
Wind Energy Conversion Br.

University of New Mexico (2)  
Albuquerque, NM 87106  
Attn: K. T. Feldman  
Energy Research Center  
V. Sloglund  
ME Department

A. V. da Rosa  
Stanford Electronic Laboratories  
Radio Science Laboratory  
Stanford, CA 94305

A. N. L. Chiu  
University of Hawaii  
Wind Engineering Research Digest  
Spalding Hall 357  
Honolulu, HI 96822

R. N. Meroney  
Colorado State University  
Dept. of Civil Engineering  
Fort Collins, CO 80521

A. G. Vacroux  
Illinois Institute of Technology  
Dept. of Electrical Engineering  
3300 South Federal  
Chicago, IL 60616

Oklahoma State University (2)  
Stillwater, OK 74074  
Attn: W. L. Hughes  
EE Department  
D. K. McLaughlin  
ME Department

Oregon State University (2)  
Cornvallis, OR 97331  
Attn: R. Wilson  
ME Department  
R. W. Thresher  
ME Department

Texas Tech University (3)  
P. O. Box 4289  
Lubbock, TX 79409  
Attn: K. C. Mehta, CE Dept.  
J. Strickland, ME Dept.  
J. Lawrence, ME Dept.

R. G. Watts  
Tulane University  
Dept. of Mechanical Engineering  
New Orleans, LA 70018

Aero Engineering Department (2)  
Wichita State University  
Wichita, KS 67208  
Attn: M. Snyder  
Bill Wentz

ERDA (2)  
Nevada Operations Office  
P. O. Box 14100  
Las Vegas, NV 89114  
Attn: R. Ray, Operations  
H. Mueller, ARL

DISTRIBUTION (cont):

Los Alamos Scientific Lab (7)  
P. O. Box 1663  
Los Alamos, NM 87544  
Attn: R. R. Brownlee, J-9  
J. R. Bartlit, Qu-26  
J. D. Balcomb, Q-DO-T  
R. G. Wagner, P-5  
J. Nachamkin, T-DO-TEC  
S. W. Depp, E-DO  
H. Deinken, ADWP-1

ERDA (3)  
ALO  
Kirtland AFB East  
Albuquerque, NM 87115  
Attn: D. K. Knowlin  
D. C. Graves  
D. W. King

R. Camerero  
Faculty of Applied Science  
University of Sherbrooke  
Sherbrooke, Quebec  
Canada J1K 2R1

American Wind Energy Association  
21243 Grand River  
Detroit, MI 48219

E. E. Anderson  
South Dakota Sch. of Mines & Tech.  
Dept. of Mechanical Engineering  
Rapid City, SD 57701

E. S. Takle  
Iowa State University  
Climatology and Meteorology  
312 Curtiss Hall  
Ames, IA 50010

P. B. S. Lissaman  
Aeroenvironment, Inc.  
660 South Arroyo Parkway  
Pasadena, CA 91105

R. A. Parmelee  
Northwestern University  
Department of Civil Engineering  
Evanston, IL 60201

J. Park  
Helion  
P. O. Box 4301  
Sylmar, CA 91342

W. F. Foshag  
Aerophysics Company  
3500 Connecticut Avenue NW  
Washington, DC 20008

W. L. Harris  
Aero/Astro Department  
MIT  
Cambridge, MA 02139

K. Bergey  
University of Oklahoma  
Aero Engineering Department  
Norman, OK 73069

J. Fischer  
F. L. Smidth & Company A/S  
Vigerslevalle 77  
2500 Valby, Denmark

H. M. Busey  
DMA, Safety and Facilities A-364  
ERDA Headquarters  
Washington, DC 20545

P. Bailey  
P. O. Box 3  
Kodiak, AK 99615

M. E. Beecher  
Arizona State University  
Solar Energy Collection  
University Library  
Tempe, AZ 85281

U. A. Coty  
Lockheed California Co.  
Box 551-63A1  
Burbank, CA 91520

Lawrence Livermore Laboratory (2)  
P. O. Box 808 L-340  
Livermore, CA 94550  
Attn: D. W. Dorn  
D. Hardy

J. A. Garate  
General Electric  
Valley Forge Space Center  
King of Prussia, PA 19406

O. Krauss  
Michigan State University  
Division of Engineering Research  
East Lansing, MI 48824

P. Calnan  
Electrical Research Associates  
Cleeve Road  
Leatherhead  
Surrey, England

V. Nelson  
West Texas State University  
Department of Physics  
P. O. Box 248  
Canyon, TX 79016

DISTRIBUTION (cont):

E. Gilmore  
Amarillo College  
Amarillo, TX 79100

L. Liljdahl  
Building 303  
Agriculture Research Center  
USDA  
Beltsville, MD 20705

T. Wentink, Jr.  
University of Alaska  
Geophysical Institute  
Fairbanks, AK 99701

E. J. Warchol  
Bonneville Power Administration  
P. O. Box 3621  
Portland, OR 97225

D. Lindley  
University of Canterbury  
Mechanical Engineering  
Christchurch, New Zealand

Olle Ljungstrom  
Swedish Board for Tech. Development  
FACK  
S-100 72 Stockholm 43, Sweden

Robert Brulle  
McDonnell-Douglas  
P. O. Box 516  
Dept. 241, Bldg. 32  
St. Louis, MO 63166

R. Walters  
W. Va. University  
Aero Engineering  
1062 Kountz Ave  
Morgantown, WV 26505

Albert Fritzsche  
Dornier System GmbH  
Postfach 1360  
7990 Friedrichshafen  
West Germany

P. N. Shankar  
Aerodynamics Division  
National Aeronautical Laboratory  
Bangalore 560017  
India

Peter Andersen  
Karstykke 42  
Vvelse 3550  
Slangerup, Denmark

Otto de Vries  
National Aerospace Laboratory  
Anthony Fokkerweg 2  
Amsterdam 1017  
The Netherlands

J. P. Johnston  
Stanford University  
Mechanical Engineering  
Stanford, CA 94305

Lt T. Colburn  
USCG R&D Center  
Avory Point  
Groton, CT 06340

James Meiggs  
Kaman Sciences Corp.  
P. O. Box 7463  
Colorado Springs, CO 80933

G. P. Hawkins  
Irwin Industries  
6045 West 55th Place  
Arvada, CO 80002

D. Greider  
Solar Central  
7213 Ridge Rd.  
Mechanicsburg, OH 43044

D. G. Shepherd  
Cornell University  
Sibley School of Mechanical and Aerospace  
Engineering  
Ithaca, NY 14853

B. Maribo Pedersen  
Dept of Fluid Mechanics  
Bldg. 404, DTH  
2800 Lyngby  
Denmark

Leo H. Soderholm  
Iowa State University  
Agricultural Engineering, Rm 213  
Ames, IA 50010

J. B. F. Scientific Corporation  
2 Jewel Drive  
Wilmington, MA 01887  
Attn: E. E. Johanson

United Nations Environment Programme  
485 Lexington Avenue  
New York, NY 10017  
Attn: I. H. Usmani

DISTRIBUTION (cont):

G. N. Monsson  
Mineral Development Geologist  
Dept. of Economic Planning and Development  
Barrett Building  
Cheyenne, WY 82002

M. Lechner  
Public Service Co. N. Mex.  
P. O. Box 2267  
Albuquerque, NM 87103

J. Lerner  
State Energy Commission  
Research and Development Division  
1111 Howe Avenue  
Sacramento, CA 95825

J. Nightingale  
1735 Hunt Avenue  
Richland, WA 99352

F. K. Bechtel  
Washington State University  
Department of Electrical Engineering  
College of Engineering  
Pullman, Washington 99163

General Electric Co. (2)  
Advanced Energy Programs  
Valley Forge Space Center  
P. O. Box 8661  
Philadelphia, PA 19101  
Attn: S. L. Macklis  
J. S. Zimmerman

Frank Matanzo  
Dardalean Associates  
15110 Frederick Road  
Woodbine, MD 21797

O. Igra  
Dept. of Mechanical Engineering  
Ben-Gurion University of the Negev  
Beer-Sheva, Israel

H. K. Skeele  
Learning Unlimited Corporation  
72 Park Street  
New Canaan, CT 06840

United Engineers and Constructors, Inc.  
Advanced Engineering Department  
30 South 17th Street  
Philadelphia, PA 19101  
Attn: A. J. Karalis,  
Manager, Special Projects

Electric Power Research Institute  
3412 Hillview Avenue  
Palo Alto, CA 94304  
Attn: P. Bos  
Program Manager, Solar Energy

D. Ham  
Massachusetts Institute of Technology  
77 Massachusetts Avenue  
Cambridge, MA 02139

Kaman Aerospace Corporation  
Old Windsor Road  
Bloomfield, CT 06002  
Attn: J. Barzda  
Chief of Systems Research

Southwest Research Institute (2)  
P. O. Drawer 28501  
San Antonio, TX 78284  
Attn: W. L. Donaldson  
Senior Vice President  
R. K. Swanson

L. H. J. Maile  
Engineering Manager  
Dominion Aluminum Fabricating Ltd.  
3570 Hawkestone Road  
Mississauga, Ontario L5C 2V8 Canada

1000 G. A. Fowler  
1200 W. A. Gardner  
1280 T. B. Lane  
1281 S. W. Key  
1281 J. H. Biffle  
1281 R. Rodeman  
1284 R. T. Othmer  
1284 W. N. Sullivan  
1284 L. I. Weingarten  
1300 D. B. Shuster  
1320 M. L. Kramm  
1324 E. C. Rightley  
1324 L. V. Feltz  
1324 D. F. McNeill  
1330 R. C. Maydew  
1333 S. McAlees, Jr.  
1333 B. F. Blackwell  
1333 R. E. Sheldahl  
1400 A. Y. Pope  
3161 J. E. Mitchell (15)  
5000 A. Narath  
5431 D. W. Lobitz  
5443 J. W. Reed  
5700 J. H. Scott  
5710 G. E. Brandvold  
5715 R. H. Braasch

Reprinted January 1980

DISTRIBUTION (cont):

5715 E. G. Kadlec (50)  
5715 R. C. Reuter  
5715 A. F. Veneruso  
5740 V. L. Dugan  
5742 S. G. Varnado  
5742 J. F. Banas  
8000 T. B. Cook, Jr.  
8100 L. Gutierrez  
8110 A. N. Blackwell  
8300 B. F. Murphey  
8320 T. S. Gold  
9486 R. C. Anderson  
9743 K. G. Grant  
8266 E. A. Aas (2)  
3141 C. A. Pepmueller (Actg.) (5)  
3151 W. L. Garner (3)  
For ERDA/TIC (Unlimited Release)

